

A Supervised Tensor Dimension Reduction-Based Prognostic Model for Applications with Incomplete Imaging Data

Chengyu Zhou

Edward P. Fitts Department of Industrial and Systems Engineering,
North Carolina State University

and

Xiaolei Fang

Edward P. Fitts Department of Industrial and Systems Engineering,
North Carolina State University

Abstract

Imaging data-based prognostic models focus on using an asset's degradation images to predict its time-to-failure (TTF). Most image-based prognostic models have two common limitations. First, they require degradation images to be complete (i.e., images are observed continuously and regularly over time). Second, they usually employ an unsupervised dimension reduction method to extract low-dimensional features, and then use the features for TTF prediction. Since unsupervised dimension reduction is conducted on the degradation images without the involvement of TTFs, there is no guarantee that the extracted features are effective for failure time prediction. To address these challenges, this article develops a supervised tensor dimension reduction-based prognostic model. The model first proposes a supervised dimension reduction method for tensor data. It uses historical TTFs to guide the detection of a tensor subspace to extract low-dimensional features from high-dimensional incomplete degradation imaging data. Next, the extracted features are used to construct a prognostic model based on (log)-location-scale regression. An optimization algorithm is proposed for parameter estimation, and closed-form solutions are derived under certain distributions. Simulated data and a real-world data set are used to validate the performance of the proposed model.

Keywords: Supervised dimension reduction, missing data, tensor, failure time prediction

1 Introduction

Degradation is an irreversible process of damage accumulation that results in the failure of engineering systems/assets/components (Bogdanoff and Kozin, 1985). Although it is usually challenging to observe a physical degradation process, there often are some manifestations associated with degradation processes that can be monitored by sensing technology, which yields data known as degradation data/signals. Degradation data contains the health condition of engineering assets; thus, if modeled properly, they can be used to predict the assets' time-to-failure (TTF) via a process known as prognostic. Many prognostic models have been developed in the literature, most of which focus on using time series-based degradation data (Ye et al., 2014; Ye and Chen, 2014; Hong and Meeker, 2010, 2013; Shu et al., 2015; Liu et al., 2013; Gebraeel et al., 2005). Recently, prognostic models with imaging-based degradation data have been investigated and attracted more and more attention (Fang et al., 2019; Aydemir and Paynabar, 2019; Yang et al., 2021; Dong et al., 2021; Tang et al., 2021; Jiang et al., 2022). This is because comparing with time-series data, imaging data usually contains much richer information of the object being monitored, and imaging sensing technologies are noncontact and thus they can usually be easily deployed. One example of imaging-based degradation data is the infrared image stream that measures the change of temperature distribution of a thrust bearing during its degradation process over time (Fang et al., 2019; Aydemir and Paynabar, 2019; Dong et al., 2021; Jiang et al., 2022). Another example is the images used to measure the performance degradation of infrared systems such as rotary-wing drones (Dong et al., 2021).

The existing imaging-based prognostic methods include deep learning-based models and statistical learning methods. Examples of the deep learning-based models designed for TTF prediction using imaging data include the ones developed by Aydemir and Paynabar (2019); Yang et al. (2021); Dong et al. (2021), and Jiang et al. (2022). Although these models have worked relatively well, they usually provide point estimations of failure times, and it is challenging for them to quantify the uncertainty of predicted TTFs. This limits their applicability since the subsequent decision-making analysis such as maintenance/inventory/logistic optimization requires prognostic models to provide a distribution of the predicted TTF. One example of statistical learning methods for image-based prog-

nostic model is the penalized (log)-location-scale (LLS) tensor regression proposed by Fang et al. (2019). The model first employs multilinear principal component analysis (MPCA) (Lu et al., 2008) to reduce the dimension of high-dimensional imaging-based degradation data, which yields a low-dimensional feature tensor for each asset. Next, it constructs a prognostic model by regressing an asset’s TTF against its low-dimensional feature tensor using LLS regression. In the same article, Fang et al. (2019) have also proposed several benchmarking prognostic models that use imaging-based degradation data for TTF prediction. These models also first employ a dimension reduction method such as functional principal component analysis (FPCA) (Ramsay and Silverman, 2005), principal component analysis (PCA) (Abdi and Williams, 2010), or B-Spline (Prautzsch et al., 2002), to reduce the dimension of degradation data and then use low-dimensional features to build an LLS regression model for prognostic. Although the aforementioned statistical learning-based prognostic models can provide a distribution for the predicted TTF, and their effectiveness have been well investigated, they share two common limitations.

The first limitation is that they assume imaging-based degradation data (including historical data for model training and real-time data for model test) are complete, which means images from all the assets should be collected continuously and regularly with the same sampling time interval (see Figure 1 (a) for an example). In reality, however, engineering assets often operate in harsh environments that significantly impact the quality of collected data due to errors in data acquisition, communication, read/write operations, etc. As a result, degradation images often contain significant levels of missing observations, which is known as incomplete/missing imaging data (see Figure 1 (b) for an example). Such data incompleteness poses a significant challenge for the parameter estimation of existing statistical learning-based prognostic models.

The second common limitation for the existing statistical learning-based prognostic models for applications with imaging data is that they employ unsupervised dimension reduction methods for feature extraction, so there is no guarantee that the extracted features are effective for the subsequent TTF prediction. Specifically, they first use unsupervised dimension reduction methods such as FPCA, PCA, and B Spline to extract features, which are then used to construct prognostic models. Since feature extraction and prognostic model construction are two sequential steps, and no TTF information gets involved in

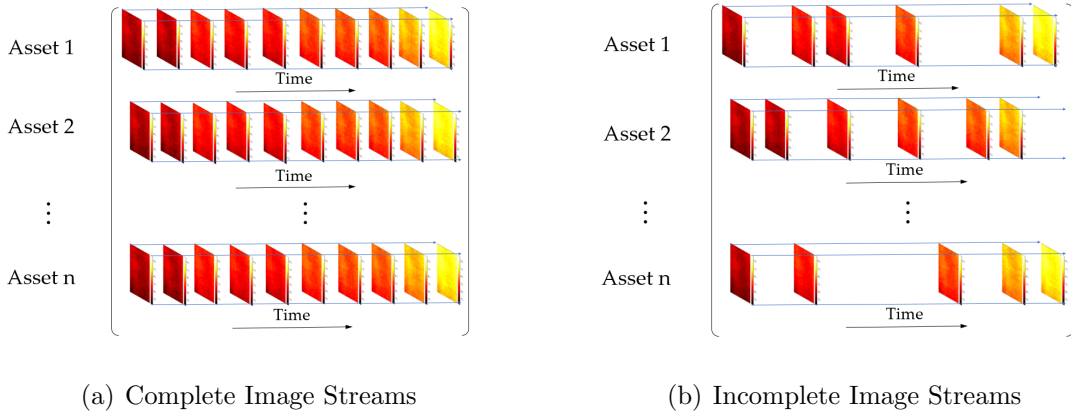


Figure 1: Degradation stream images with and without missing data.

the feature extraction process, it is possible that the extracted features may not be most suitable for predicting TTFs.

To address the aforementioned challenges, this article proposes a supervised dimension reduction-based prognostic model that uses an asset’s incomplete degradation images to predict its TTF. Similar to the existing statistical learning-based prognostic models, the proposed model also consists of two steps: feature extraction and prognostic model construction. However, **unlike the existing models, feature extraction in this article is achieved by developing a new supervised tensor dimension reduction method, which uses historical TTFs to supervise the feature extraction process such that the extracted features are more effective for the subsequent TTF prediction.** In addition, **unlike the existing unsupervised dimension reduction methods that only work for complete imaging data, the proposed supervised dimension reduction method works for both complete and incomplete degradation image streams.**

The proposed supervised dimension reduction method works as follows: First, it detects a low-dimensional tensor subspace in which the high-dimensional degradation image streams are embedded. This is achieved by constructing an optimization criterion that comprises a feature extraction term and a regression term. The first term extracts low-dimensional features from complete/incomplete degradation image streams of training assets, and the second term builds the connection between these assets’ TTFs and the extracted features using LLS regression. LLS regression has been widely used in reliabil-

ity engineering and survival analysis. It includes a variety of TTF distributions, such as (log)normal, (log)logistic, smallest extreme value, and Weibull, etc., which cover most of the TTF distributions in reality (Doray, 1994). Since historical TTFs are used to supervise the feature extraction process, it is expected that the extracted features are more effective for the subsequent prognostic. Solving the optimization criterion of the proposed supervised tensor dimension reduction method yields a set of tensor basis matrices that span the low-dimensional tensor subspace for dimension reduction. We then expand both the historical degradation images in the training data set and real-time degradation images from an asset operating in the field (i.e., test data) using the set of tensor basis matrices to extract the low-dimensional tensor features of the training assets and the test asset. The TTFs of the training assets are then regressed against their tensor features using LLS regression, and the parameters are estimated using maximum likelihood estimation. After that, the tensor features of the test asset are fed into the LLS regression model, and its TTF distribution is predicted.

To solve the optimization criterion of the proposed supervised dimension reduction method, we will first transfer the criterion into a block multiconvex problem. Next, we will propose a block updating algorithm, which cyclically optimizes one block parameters while keeping other blocks fixed until convergence. In addition, we will demonstrate that when TTFs follow normal or lognormal distributions, each sub problem of the block updating algorithm has a closed-form solution, no matter the degradation image streams are complete or incomplete.

The rest of this paper is organized as follows. Section 2 presents the supervised tensor dimension reduction-based prognostic method. Section 3 introduces the block updating algorithm and closed-form solutions when TTFs follow normal/lognormal distributions. Sections 5 and 6 validate the effectiveness of the proposed prognostic model using a simulated dataset and data from a rotating machinery, respectively. Section 7 concludes.

2 The Methodology

In this section, we will introduce the proposed supervised tensor dimension reduction-based prognostic model for applications with incomplete imaging data. In Subsection 2.1,

we will present some basic tensor notations and definitions. Subsection 2.2 introduces the supervised tensor dimension reduction method. In Subsection 2.3, we will discuss the construction of prognostic model and how to predict the TTF of an asset operating in the field using its real-time degradation imaging data.

2.1 Preliminaries

In this section, we introduce some basic notations and definitions of tensor operations that are used throughout the article. The *order* of a tensor is the number of dimensions, also known as ways or modes. Vectors (1 order tensors) are denoted by lowercase boldface letters, e.g., \mathbf{s} . Matrices (2 order tensors) are denoted by boldface uppercase letters, e.g., \mathbf{S} . Higher-order tensors (order is 3 or larger) are denoted by calligraphic letters, e.g., \mathcal{S} . Indices are denoted by lowercase letters whose range is from 1 to the uppercase letter of the index, e.g., $n = 1, 2, \dots, N$. An N th-order tensor is denoted as $\mathcal{S} \in \mathbb{R}^{I_1 \times I_2 \times \dots \times I_N}$, where I_n represents the n th mode of \mathcal{S} . The (i_1, i_2, \dots, i_N) th entry of $\mathcal{S} \in \mathbb{R}^{I_1 \times I_2 \times \dots \times I_N}$ is denoted by s_{i_1, i_2, \dots, i_N} . A fiber of \mathcal{S} is a vector defined by fixing every index but one. A matrix column is a mode-1 fiber and a matrix row is a mode-2 fiber. The *vectorization* of \mathcal{S} , denoted by $\text{vec}(\mathcal{S})$, stacks all the entries of \mathcal{S} into a column vector. The *mode- n matricization* of a tensor $\mathcal{S} \in \mathbb{R}^{I_1 \times I_2 \times \dots \times I_N}$ is denoted by $\mathbf{S}_{(n)}$, which arranges the mode- n fibers to be the columns of the resulting matrix. The n th mode product of a tensor $\mathcal{S} \in \mathbb{R}^{I_1 \times I_2 \times \dots \times I_N}$ and a matrix $\mathbf{U}_n \in \mathbb{R}^{J_n \times I_n}$, denoted by $\mathcal{S} \times_n \mathbf{U}_n$, is a tensor whose entry is $(\mathcal{S} \times_n \mathbf{U}_n)_{i_1, \dots, i_{n-1}, j_n, i_{n+1}, \dots, i_N} = \sum_{I_n=1}^{I_n} s_{i_1, \dots, i_N} u_{j, i_n}$. The *Kronecker product* of two matrices $\mathbf{A} \in \mathbb{R}^{m \times n}$ and $\mathbf{B} \in \mathbb{R}^{p \times q}$ is an $mp \times nq$ block matrix:

$$\mathbf{A} \otimes \mathbf{B} = \begin{bmatrix} \mathbf{a}_{11}\mathbf{B} & \dots & \mathbf{a}_{1n}\mathbf{B} \\ \vdots & \ddots & \vdots \\ \mathbf{a}_{m1}\mathbf{B} & \dots & \mathbf{a}_{mn}\mathbf{B} \end{bmatrix}.$$

If \mathbf{A} and \mathbf{B} have the same number of columns $n = q$, then the *Khatri-Rao* product is defined as the $mp \times n$ column-wise *Kronecker* product: $\mathbf{A} \odot \mathbf{B} = [\mathbf{a}_1 \otimes \mathbf{b}_1 \quad \mathbf{a}_2 \otimes \mathbf{b}_2 \quad \dots \quad \mathbf{a}_n \otimes \mathbf{b}_n]$. If \mathbf{a} and \mathbf{b} are vectors, then $\mathbf{A} \otimes \mathbf{B} = \mathbf{A} \odot \mathbf{B}$. More details about tensor notations and operators can be found in Kolda and Bader (2009).

2.2 The Supervised Tensor Dimension Reduction Method

We assume that there exists a historical data set for model training. The data set consists of the degradation image streams of M failed assets along with their TTFs, which are denoted as $\mathcal{X}_m \in \mathbb{R}^{I_1 \times I_2 \times I_3}$ and $y_m \in \mathbb{R}$, respectively, where $m = 1, 2, \dots, M$. For the convenience of introducing the dimension reduction method, we convert the 3D degradation image streams from all the M assets to a 4D tensor $\mathcal{X} \in \mathbb{R}^{I_1 \times I_2 \times I_3 \times M}$, where the sample size M is the 4th mode. Similarly, we let $\mathbf{y} = (y_1, \dots, y_M)^\top \in \mathbb{R}^{M \times 1}$ be the vector containing all the TTFs of the M assets.

Out of the $I_1 \times I_2 \times I_3 \times M$ entries of \mathcal{X} , we use a subset $\Omega \subseteq \{(i_1, i_2, i_3, m), 1 \leq i_1 \leq I_1, 1 \leq i_2 \leq I_2, 1 \leq i_3 \leq I_3, 1 \leq m \leq M\}$ to denote the indices of the missing ones. To model the missing data, we define a projection operator $\mathcal{P}_\Omega(\cdot)$ as follows:

$$\mathcal{P}_\Omega(\mathcal{X})_{(i_1, i_2, i_3, m)} = \begin{cases} \mathcal{X}_{(i_1, i_2, i_3, m)}, & \text{if } (i_1, i_2, i_3, m) \notin \Omega, \\ 0, & \text{if } (i_1, i_2, i_3, m) \in \Omega, \end{cases} \quad (1)$$

where $\mathcal{X}_{(i_1, i_2, i_3, m)}$ is the (i_1, i_2, i_3, m) -th entry of the 4D tensor $\mathcal{X} \in \mathbb{R}^{I_1 \times I_2 \times I_3 \times M}$. To recover the missing entries in tensor \mathcal{X} , we may employ the following Tucker decomposition-based tensor completion method (Filipović and Jukić, 2015; Liu et al., 2012; Xu et al., 2013):

$$\min_{\mathcal{S}, \mathbf{U}_1, \mathbf{U}_2, \mathbf{U}_3} \|\mathcal{P}_\Omega(\mathcal{X} - \mathcal{S} \times_1 \mathbf{U}_1^\top \times_2 \mathbf{U}_2^\top \times_3 \mathbf{U}_3^\top)\|_F^2. \quad (2)$$

where $\|\cdot\|_F^2$ is the Frobenius norm, $\mathbf{U}_1 \in \mathbb{R}^{P_1 \times I_1}$, $\mathbf{U}_2 \in \mathbb{R}^{P_2 \times I_2}$, $\mathbf{U}_3 \in \mathbb{R}^{P_3 \times I_3}$ are three factor matrices, $\mathcal{S} \in \mathbb{R}^{P_1 \times P_2 \times P_3 \times M}$ is the low-dimensional core tensor, and \times_n is the n -mode product of a tensor with a matrix. The tensor completion criterion (2) can be seen as an *unsupervised dimension reduction method* for tensor data with missing entries. This is because the degradation image tensor $\mathcal{X} \in \mathbb{R}^{I_1 \times I_2 \times I_3 \times M}$ is a 4-order tensor, which resides in the tensor (multilinear) space $\mathbb{R}^{I_1} \otimes \mathbb{R}^{I_2} \otimes \mathbb{R}^{I_3} \otimes \mathbb{R}^M$, where $\mathbb{R}^{I_1}, \mathbb{R}^{I_2}, \mathbb{R}^{I_3}, \mathbb{R}^M$ are the 4 vector (linear) spaces; $\mathcal{S} \in \mathbb{R}^{P_1 \times P_2 \times P_3 \times M}$ can be seen as a feature tensor that resides in the tensor space $\mathbb{R}^{P_1} \otimes \mathbb{R}^{P_2} \otimes \mathbb{R}^{P_3} \otimes \mathbb{R}^M$. Usually, we have $P_1 \ll I_1$, $P_2 \ll I_2$, and $P_3 \ll I_3$ for degradation imaging data due to the high spatio-temporal correlation among the pixels. This implies that the dimension of the image stream from the m th asset is reduced from $\mathbb{R}^{I_1 \times I_2 \times I_3}$ to $\mathbb{R}^{P_1 \times P_2 \times P_3}$, where $m = 1, \dots, M$.

Although criterion (2) can be seen as a dimension reduction method, there is no guarantee that the extracted low-dimensional feature tensor \mathcal{S} is effective for the subsequent TTF prediction. To address this challenge, we propose the following *supervised dimension reduction* method by combining a tensor completion term and an LLS regression term:

$$\min_{\mathbf{U}_1, \mathbf{U}_2, \mathbf{U}_3, \beta_1, \beta_0, \mathcal{S}} \alpha \|\mathcal{P}_\Omega(\mathcal{X} - \mathcal{S} \times_1 \mathbf{U}_1^\top \times_2 \mathbf{U}_2^\top \times_3 \mathbf{U}_3^\top)\|_F^2 + (1 - \alpha) \ell\left(\frac{\mathbf{y} - \mathbf{1}_M \beta_0 - \mathbf{S}_{(4)} \beta_1}{\sigma}\right), \quad (3)$$

where $\mathbf{y} \in \mathbb{R}^{M \times 1}$ is the vector containing all the TTFs of the M assets in the training data set. The matrix $\mathbf{S}_{(4)} \in \mathbb{R}^{M \times (P_1 \times P_2 \times P_3)}$ is the mode-4 matricization of the low-dimensional feature tensor \mathcal{S} , the m th row of which represents the vectorization of the m th asset's feature tensor, $m = 1, \dots, M$. β_0 is the intercept, and $\beta_1 \in \mathbb{R}^{(P_1 \times P_2 \times P_3) \times 1}$ is the regression coefficient vector. $\mathbf{1}_m \in \mathbb{R}^{M \times 1}$ is an $M \times 1$ vector whose elements are all ones. $\ell(\cdot)$ is the negative log-likelihood function of a location-scale distribution. For example, if TTFs follow normal distributions, then $\ell\left(\frac{\mathbf{y} - \mathbf{1}_M \beta_0 - \mathbf{S}_{(4)} \beta_1}{\sigma}\right) = \frac{M}{2} \log 2\pi + M \log \sigma + \frac{1}{2} \sum_{m=1}^M \omega_m^2$, where $\omega_m = \frac{y_m - \beta_0 - \mathbf{s}_{(4)}^m}{\sigma}$, where $\mathbf{s}_{(4)}^m$ is the m th row of $\mathbf{S}_{(4)}$, and y_m is the TTF of asset m ; if TTFs follow logistic distributions, then $\ell\left(\frac{\mathbf{y} - \mathbf{1}_M \beta_0 - \mathbf{S}_{(4)} \beta_1}{\sigma}\right) = M \log \sigma - \sum_{m=1}^M \omega_m + 2 \sum_{m=1}^M \log(1 + \exp(\omega_m))$; if TTFs follow small extreme value (SEV) distributions, then $\ell\left(\frac{\mathbf{y} - \mathbf{1}_M \beta_0 - \mathbf{S}_{(4)} \beta_1}{\sigma}\right) = n \log \sigma - \sum_{m=1}^M \omega_m + \sum_{m=1}^M \exp(\omega_m)$. For assets whose TTFs follow log-location-scale distributions, we may transfer them to the corresponding location-scale distributions by taking their logarithm such that criterion (3) can still be used. For example, log-normal, log-logistics, and Weibull distributions can be transferred to normal, logistics, and SEV distributions, respectively. $\alpha \in [0, 1]$ is a weight and $\|\cdot\|_F^2$ is the Frobenius norm.

In criterion (3), the first term $\|\mathcal{P}_\Omega(\mathcal{X} - \mathcal{S} \times_1 \mathbf{U}_1^\top \times_2 \mathbf{U}_2^\top \times_3 \mathbf{U}_3^\top)\|_F^2$ is tensor completion from (2), which reduces the dimension of high-dimensional incomplete degradation image streams and extracts low-dimensional tensor features. The second term $\ell\left(\frac{\mathbf{y} - \mathbf{1}_M \beta_0 - \mathbf{S}_{(4)} \beta_1}{\sigma}\right)$ is LLS regression, which regresses each asset's TTF against its tensor features extracted by the first term. By jointly optimizing the two terms, it is expected that the extracted features are effective for TTF prediction. However, it is challenging to solve criterion (3) since it is neither convex nor block multi-convex. An optimization problem is block multi-convex when its feasible set and objective function are generally non-convex but convex in each block of variables (Xu and Yin, 2013). Thus, to simplify the development of optimization algorithms for model parameter estimation, we first transform criterion (3)

to be a block multi-convex one. Specifically, we apply the following re-parameterization: $\tilde{\sigma} = 1/\sigma$, $\tilde{\beta}_0 = \beta_0/\sigma$, $\tilde{\beta}_1 = \beta_1/\sigma$. As a result, criterion (3) can be re-expressed as follows:

$$\min_{\mathbf{U}_1, \mathbf{U}_2, \mathbf{U}_3, \tilde{\beta}_1, \tilde{\beta}_0, \mathbf{S}_{(4)}} \alpha \|\mathcal{P}_\Omega(\mathcal{X} - \mathbf{S} \times_1 \mathbf{U}_1^\top \times_2 \mathbf{U}_2^\top \times_3 \mathbf{U}_3^\top)\|_F^2 + (1 - \alpha) \ell(\tilde{\sigma} \mathbf{y} - \mathbf{1}_M \tilde{\beta}_0 - \mathbf{S}_{(4)} \tilde{\beta}_1), \quad (4)$$

where, $\ell(\tilde{\sigma} \mathbf{y} - \mathbf{1}_M \tilde{\beta}_0 - \mathbf{S}_{(4)} \tilde{\beta}_1) = \frac{M}{2} \log 2\pi - M \log \tilde{\sigma} + \frac{1}{2} \sum_{m=1}^M \tilde{\omega}_m^2$ for TTFs following normal distributions, and $\tilde{\omega}_m = \tilde{\sigma} y_m - \tilde{\beta}_0 - \mathbf{s}_{(4)}^m$, where $\mathbf{s}_{(4)}^m$ is the m th row of $\mathbf{S}_{(4)}$ and y_m is the TTF of asset m ; $\ell(\tilde{\sigma} \mathbf{y} - \mathbf{1}_M \tilde{\beta}_0 - \mathbf{S}_{(4)} \tilde{\beta}_1) = -M \log \tilde{\sigma} - \sum_{m=1}^M \tilde{\omega}_m + 2 \sum_{m=1}^M \log(1 + \exp(\tilde{\omega}_m))$ for TTFs following logistics distributions, and $\ell(\tilde{\sigma} \mathbf{y} - \mathbf{1}_M \tilde{\beta}_0 - \mathbf{S}_{(4)} \tilde{\beta}_1) = -n \log \tilde{\sigma} - \sum_{m=1}^M \tilde{\omega}_m + \sum_{m=1}^M \exp(\tilde{\omega}_m)$ for TTFs following SEV distributions.

The optimization algorithm to solve criterion (4) will be discussed later in Section 3. The value of the weight α and the dimension of the low-dimensional tensor subspace $\{P_1, P_2, P_3\}$ can be determined using a model selection method such as cross-validation. Solving the optimization criterion (4) using historical training data yields a set of basis matrices $\hat{\mathbf{U}}_1 \in \mathbb{R}^{P_1 \times I_1}$, $\hat{\mathbf{U}}_2 \in \mathbb{R}^{P_2 \times I_2}$, $\hat{\mathbf{U}}_3 \in \mathbb{R}^{P_3 \times I_3}$, which contains P_1 basis vectors of the 1-mode linear space \mathbb{R}^{I_1} , P_2 basis vectors of the 2-mode linear space \mathbb{R}^{I_2} , and P_3 basis vectors of the 3-mode linear space \mathbb{R}^{I_3} , respectively. The three linear subspaces form the low-dimensional tensor subspace $\mathbb{R}^{P_1} \otimes \mathbb{R}^{P_2} \otimes \mathbb{R}^{P_3}$ detected by the proposed supervised dimension reduction method.

2.3 Prognostic Model Construction and Real-Time TTF Prediction

In this subsection, we discuss how to build a prognostic model based on the supervised dimension reduction method proposed in Section 2.2, and how to predict the TTF distribution of an asset operating in the field using its real-time degradation image data.

Similar to Section 2.2, we denote the training data set as $\{\mathcal{X}_m \in \mathbb{R}^{I_1 \times I_2 \times D_m}, y_m\}_{m=1}^M$, where M is the number of failed assets in the training data set. Notice that D_m might not be the same as $D_{m'}$ for two assets m and m' , $m = 1, \dots, M$, $m' = 1, \dots, M$, $m \neq m'$. This is because different asset's failure times (i.e., TTFs) are different, and usually no image data can be collected beyond an asset's failure time since the asset is stopped for maintenance or replace once it is failed. In addition to the training data, we denote the degradation image

stream of a test asset by time t as $\mathcal{X}_t \in \mathbb{R}^{I_1 \times I_2 \times I_t}$. The objectives of this subsection include 1) constructing a prognostic model and estimating its parameters using $\{\mathcal{X}_m, y_m\}_{m=1}^M$ in the training data set, and 2) using the estimated prognostic model to predict the TTF (denoted as \hat{y}_t) of the test asset based on its degradation image stream \mathcal{X}_t .

We first use the proposed supervised dimension reduction method to extract low-dimensional features of both the training and test assets. Specifically, as discussed in Section 2.2, we first construct a 4D tensor $\mathcal{X} \in \mathbb{R}^{I_1 \times I_2 \times I_3 \times M}$ using the degradation image streams of the training assets, where $I_3 = \max(\{D_m\}_{m=1}^M)$. Note that \mathcal{X} is an incomplete tensor no matter the image streams from the training assets are complete or incomplete. This is because the TTFs of training assets are different, and thus not all the training assets have I_3 images. To detect the low-dimensional tensor subspace in which the high-dimensional degradation images are embedded, we solve optimization criterion (4) by using training data $\{\mathcal{X}, \mathbf{y}\}$, where $\mathbf{y} = (y_1, \dots, y_M)^\top$. This yields basis matrices $\hat{\mathbf{U}}_1 \in \mathbb{R}^{P_1 \times I_1}$, $\hat{\mathbf{U}}_2 \in \mathbb{R}^{P_2 \times I_2}$, $\hat{\mathbf{U}}_3 \in \mathbb{R}^{P_3 \times I_3}$, which form the low-dimensional tensor subspace $\mathbb{R}^{P_1} \otimes \mathbb{R}^{P_2} \otimes \mathbb{R}^{P_3}$. To extract the low-dimensional features of the training and test assets, we expand the image streams in the low-dimensional tensor subspace $\mathbb{R}^{P_1} \otimes \mathbb{R}^{P_2} \otimes \mathbb{R}^{P_3}$ using the basis matrices $\hat{\mathbf{U}}_1, \hat{\mathbf{U}}_2, \hat{\mathbf{U}}_3$. This is achieved by solving the following optimization criteria:

$$\hat{\mathcal{S}}_m = \arg \min_{\mathcal{S}_m} \|\mathcal{P}_\Omega(\mathcal{X}_m - \mathcal{S}_m \times_1 \mathbf{U}_1^\top \times_2 \mathbf{U}_2^\top \times_3 \mathbf{U}_3^\top)\|_F^2. \quad (5)$$

$$\hat{\mathcal{S}}_t = \arg \min_{\mathcal{S}_t} \|\mathcal{P}_\Omega(\mathcal{X}_t - \mathcal{S}_t \times_1 \mathbf{U}_1^\top \times_2 \mathbf{U}_2^\top \times_3 \mathbf{U}_3^\top)\|_F^2, \quad (6)$$

where $\{\hat{\mathcal{S}}_m\}_{m=1}^M$ are the low-dimensional feature tensors of the M assets in the training data set, and $\hat{\mathcal{S}}_t$ is the low-dimensional feature tensor of the test asset.

Next, we construct a prognostic model using the low-dimensional feature tensors of the M assets in the training data set (i.e., $\{\hat{\mathcal{S}}_m\}_{m=1}^M$) along with their TTFs $\{y_m\}_{m=1}^M$. Specifically, we build the following LLS regression model:

$$y_m = \gamma_0 + \text{vec}(\hat{\mathcal{S}}_m)^\top \boldsymbol{\gamma}_1 + \sigma \epsilon_m, \quad (7)$$

where $\text{vec}(\hat{\mathcal{S}}_m)$ is the vectorization of $\hat{\mathcal{S}}_m$. $\gamma_0 \in \mathbb{R}$ and $\boldsymbol{\gamma}_1 \in \mathbb{R}^{(P_1 \times P_2 \times P_3) \times 1}$ are the regression coefficients, σ is the scale parameter, and ϵ_m is the random noise term with a standard location-scale probability density function $f(\epsilon)$. For example, $f(\epsilon) = 1/\sqrt{2\pi} \exp(-\epsilon^2/2)$ for

a normal distribution and $f(\epsilon) = \exp(\epsilon - \exp(\epsilon))$ for an SEV distribution. The parameters in criterion (7) can be estimated by solving the following optimization problem:

$$\min_{\mathbf{y}, \gamma_0, \gamma_1, \sigma} \ell\left(\frac{\mathbf{y} - \mathbf{1}_M \gamma_0 - \hat{\mathbf{S}}_{(4)} \gamma_1}{\sigma}\right), \quad (8)$$

where $\ell(\cdot)$ is the negative log-likelihood function of a location-scale distribution, $\mathbf{y} = (y_1, y_2, \dots, y_m)^\top$ and $\hat{\mathbf{S}}_{(4)} = (\text{vec}(\hat{\mathbf{S}}_1)^\top, \text{vec}(\hat{\mathbf{S}}_2)^\top, \dots, \text{vec}(\hat{\mathbf{S}}_M)^\top)^\top$, and $\ell(\cdot)$ is the negative log-likelihood function. We conduct the following reparameterization to transform the optimization to be a convex one: $\tilde{\sigma} = 1/\sigma$, $\tilde{\gamma}_0 = \gamma_0/\sigma$, $\tilde{\gamma}_1 = \gamma_1/\sigma$:

$$\{\hat{\tilde{\gamma}}_0, \hat{\tilde{\gamma}}_1, \hat{\tilde{\sigma}}\} = \arg \min_{\tilde{\gamma}_0, \tilde{\gamma}_1, \tilde{\sigma}} \ell(\tilde{\sigma} \mathbf{y} - \mathbf{1}_M \tilde{\gamma}_0 - \hat{\mathbf{S}}_{(4)} \tilde{\gamma}_1). \quad (9)$$

Solving (9) provides the estimated parameters $\{\hat{\tilde{\gamma}}_0, \hat{\tilde{\gamma}}_1, \hat{\tilde{\sigma}}\}$, which can be transformed back to the estimation of the parameters in the LLS regression model: $\hat{\gamma}_0 = \hat{\tilde{\gamma}}_0/\hat{\tilde{\sigma}}$, $\hat{\gamma}_1 = \hat{\tilde{\gamma}}_1/\hat{\tilde{\sigma}}$ and $\hat{\sigma} = 1/\hat{\tilde{\sigma}}$. As a result, the fitted LLS regression model is $\hat{y}_m \sim LLS(\hat{\gamma}_0 + \text{vec}(\hat{\mathbf{S}}_m)^\top \hat{\gamma}_1, \hat{\sigma})$, where $\hat{\gamma}_0 + \text{vec}(\hat{\mathbf{S}}_m)^\top \hat{\gamma}_1$ and $\hat{\sigma}$ are respectively the estimated location and scale parameters.

Finally, we fed the extracted low-dimensional feature tensor of the test asset into the estimated LLS regression model to predict the asset's TTF distribution: $\hat{y}_t \sim LLS(\hat{\gamma}_0 + \text{vec}(\hat{\mathbf{S}}_t)^\top \hat{\gamma}_1, \hat{\sigma})$.

3 The Optimization Algorithm for General LLS Distributions

In this section, we develop a Block Updating Algorithm to solve the supervised tensor dimension reduction method proposed in Section 2.2. The algorithm splits the unknown parameters in criterion (4) into several blocks, and it cyclically optimizes one block parameters in criterion (4) while keeping other blocks fixed until convergence. The sub optimization problem for each block is convex, so the convergence of the block updating algorithm is guaranteed. In addition, we will show that if TTFs follow normal (or log-normal) distributions, the sub optimization problem for each block has a closed-form solution, no matter the degradation image streams are complete or incomplete.

3.1 The Block Updating Algorithm for General LLS Distributions

The Block Updating Algorithm first splits the unknown parameters in criterion (4) into 5 blocks, i.e., $\mathbf{U}_1, \mathbf{U}_2, \mathbf{U}_3, \mathcal{S}$, and $\{\tilde{\beta}_0, \tilde{\beta}_1\}$. It then cyclically optimizes one block of parameters each time while keeping other blocks fixed.

Specifically, at the k th iteration, \mathbf{U}_1 is updated by solving the following optimization problem while keeping other blocks (i.e., $\mathbf{U}_2^{k-1}, \mathbf{U}_3^{k-1}, \tilde{\beta}_0^{k-1}, \tilde{\beta}_1^{k-1}, \mathcal{S}^{k-1}$) fixed:

$$\begin{aligned} \mathbf{U}_1^k = \arg \min_{\mathbf{U}_1} \quad & \alpha \|\mathcal{P}_\Omega(\mathcal{X} - \mathcal{S}^{k-1} \times_1 \mathbf{U}_1^\top \times_2 \mathbf{U}_2^{k-1\top} \times_3 \mathbf{U}_3^{k-1\top})\|_F^2 \\ & + (1 - \alpha) \ell(\tilde{\beta}_0^{k-1}, \tilde{\beta}_1^{k-1}, \mathcal{S}_{(4)}^{k-1}) \end{aligned} \quad (10)$$

Similarly, the remaining blocks are updated as follows:

$$\begin{aligned} \mathbf{U}_2^k = \arg \min_{\mathbf{U}_2} \quad & \alpha \|\mathcal{P}_\Omega(\mathcal{X} - \mathcal{S}^{k-1} \times_1 \mathbf{U}_1^{k\top} \times_2 \mathbf{U}_2^\top \times_3 \mathbf{U}_3^{k-1\top})\|_F^2 \\ & + (1 - \alpha) \ell(\tilde{\beta}_0^{k-1}, \tilde{\beta}_1^{k-1}, \mathcal{S}_{(4)}^{k-1}) \end{aligned} \quad (11)$$

$$\begin{aligned} \mathbf{U}_3^k = \arg \min_{\mathbf{U}_3} \quad & \alpha \|\mathcal{P}_\Omega(\mathcal{X} - \mathcal{S}^{k-1} \times_1 \mathbf{U}_1^{k\top} \times_2 \mathbf{U}_2^{k\top} \times_3 \mathbf{U}_3^\top)\|_F^2 \\ & + (1 - \alpha) \ell(\tilde{\beta}_0^{k-1}, \tilde{\beta}_1^{k-1}, \mathcal{S}_{(4)}^{k-1}) \end{aligned} \quad (12)$$

$$\begin{aligned} \{\tilde{\beta}_0^k, \tilde{\beta}_1^k\} = \arg \min_{\tilde{\beta}_0, \tilde{\beta}_1} \quad & \alpha \|\mathcal{P}_\Omega(\mathcal{X} - \mathcal{S}^{k-1} \times_1 \mathbf{U}_1^{k\top} \times_2 \mathbf{U}_2^{k\top} \times_3 \mathbf{U}_3^{k\top})\|_F^2 \\ & + (1 - \alpha) \ell(\tilde{\beta}_0, \tilde{\beta}_1, \mathcal{S}_{(4)}^{k-1}) \end{aligned} \quad (13)$$

$$\begin{aligned} \mathcal{S}^k = \arg \min_{\mathcal{S}} \quad & \alpha \|\mathcal{P}_\Omega(\mathcal{X} - \mathcal{S} \times_1 \mathbf{U}_1^{k\top} \times_2 \mathbf{U}_2^{k\top} \times_3 \mathbf{U}_3^{k\top})\|_F^2 \\ & + (1 - \alpha) \ell(\tilde{\beta}_0^k, \tilde{\beta}_1^k, \mathcal{S}_{(4)}) \end{aligned} \quad (14)$$

We summarize the Block Updating Algorithm in Algorithm 1 below. The convergence criterion can be set as $\Psi(\mathbf{U}_1^k, \mathbf{U}_2^k, \mathbf{U}_3^k, \tilde{\beta}_0^k, \tilde{\beta}_1^k, \mathcal{S}^k) - \Psi(\mathbf{U}_1^{k+1}, \mathbf{U}_2^{k+1}, \mathbf{U}_3^{k+1}, \tilde{\beta}_0^{k+1}, \tilde{\beta}_1^{k+1}, \mathcal{S}^{k+1}) < \epsilon$, where Ψ is the value of the objective function in criterion (4), and ϵ is a small number. It is easy to show that all the sub problems (10), (11), (12), (13), and (14) are convex. Thus, the Block Updating Algorithm converges to a stationary point of criterion (4).

The initialization of Algorithm 1 can be conducted randomly or heuristically. In this article, we propose a heuristic initialization method. Specifically, MPCA (Lu et al., 2008) is applied to tensor \mathcal{X} , which provides $\{\mathbf{U}_1^0, \mathbf{U}_2^0, \mathbf{U}_3^0\}$. Next, we compute \mathcal{S}^0 by solving $\mathcal{S}^0 = \arg \min_{\mathcal{S}} \|\mathcal{P}_\Omega(\mathcal{X} - \mathcal{S} \times_1 \mathbf{U}_1^{0\top} \times_2 \mathbf{U}_2^{0\top} \times_3 \mathbf{U}_3^{0\top})\|_F^2$. Finally, $\tilde{\beta}_0^0, \tilde{\beta}_1^0$ are computed by solving

Algorithm 1: Block Updating Algorithm for solving criterion (4)

- 1 **Input:** Tensor \mathcal{X} constructed from the (incomplete) degradation image streams of M assets and the TTF vector \mathbf{y} ; the dimension of the low-dimensional tensor subspace $\{P_1, P_2, P_3\}$
 - 2 **Initialization:** Initialize $(\mathbf{U}_1^0, \mathbf{U}_2^0, \mathbf{U}_3^0, \tilde{\beta}_0^0, \tilde{\beta}_1^0, \mathcal{S}^0)$ randomly or heuristically
 - 3 **While** convergence criterion not met **do**
 - 4 $\mathbf{U}_1^k \leftarrow (10)$
 - 5 $\mathbf{U}_2^k \leftarrow (11)$
 - 6 $\mathbf{U}_3^k \leftarrow (12)$
 - 7 $(\tilde{\beta}_0^k, \tilde{\beta}_1^k) \leftarrow (13)$
 - 8 $\mathcal{S}^k \leftarrow (14)$
 - 9 $k = k + 1$
 - 10 **End While**
 - 11 **Output:** Basis matrices of the low-dimensional tensor subspace $\{\mathbf{U}_1^k, \mathbf{U}_2^k, \mathbf{U}_3^k\}$
-

$\min_{\tilde{\beta}_0^0, \tilde{\beta}_1^0, \tilde{\sigma}} \ell(\tilde{\sigma}\mathbf{y} - \mathbf{1}_M \tilde{\beta}_0^0 - \mathbf{S}_{(4)}^0 \tilde{\beta}_1^0)$, where $\mathbf{S}_{(4)}^0$ is the mode-4 matricization of \mathcal{S}^0 . Algorithm 1 requires the dimension of the tensor subspace $\{P_1, P_2, P_3\}$ to be known in advance. This can be seen as a model selection problem such that the values of $\{P_1, P_2, P_3\}$ can be determined using cross-validation. To be specific, we may try a certain number of candidate values for $\{P_1, P_2, P_3\}$ to run Algorithm 1 to extract low-dimensional features, which are then used to build the prognostic model discussed in Section 2.3 for TTF prediction. The values which achieve the smallest prediction error will be chosen. It is known that there usually exists high spatio-temporal correlations among the degradation image streams (Fang et al., 2019), so the dimension of the tensor subspace is usually low, which helps reduce the computation intensity of model selection.

4 Closed-Form Solutions for Normal (or Lognormal) Distributions

In this section, we discuss the closed-form solutions for sub problems (10), (11), (12), (13), and (14) for applications whose assets' TTFs follow normal (or lognormal) distributions. Specifically, if the TTFs follow normal (or lognormal) distributions, we may replace the log-likelihood function-based loss function in criterion (4) with the mean squared errors. As a result, criteria (10), (11), (12),(13), and (14) can be re-expressed as follows:

$$\begin{aligned} \mathbf{U}_1^k = \arg \min_{\mathbf{U}_1} \quad & \alpha \|\mathcal{P}_\Omega(\mathcal{X} - \mathcal{S}^{k-1} \times_1 \mathbf{U}_1^\top \times_2 \mathbf{U}_2^{k-1\top} \times_3 \mathbf{U}_3^{k-1\top})\|_F^2 \\ & + (1 - \alpha) \|\mathbf{y} - \mathbf{1}_M \tilde{\beta}_0^{k-1} - \mathbf{S}_{(4)}^{k-1} \tilde{\beta}_1^{k-1}\|_2^2 \end{aligned} \quad (15)$$

$$\begin{aligned} \mathbf{U}_2^k = \arg \min_{\mathbf{U}_2} \quad & \alpha \|\mathcal{P}_\Omega(\mathcal{X} - \mathcal{S}^{k-1} \times_1 \mathbf{U}_1^{k\top} \times_2 \mathbf{U}_2^\top \times_3 \mathbf{U}_3^{k-1\top})\|_F^2 \\ & + (1 - \alpha) \|\mathbf{y} - \mathbf{1}_M \tilde{\beta}_0^{k-1} - \mathbf{S}_{(4)}^{k-1} \tilde{\beta}_1^{k-1}\|_2^2 \end{aligned} \quad (16)$$

$$\begin{aligned} \mathbf{U}_3^k = \arg \min_{\mathbf{U}_3} \quad & \alpha \|\mathcal{P}_\Omega(\mathcal{X} - \mathcal{S}^{k-1} \times_1 \mathbf{U}_1^{k\top} \times_2 \mathbf{U}_2^{k\top} \times_3 \mathbf{U}_3^\top)\|_F^2 \\ & + (1 - \alpha) \|\mathbf{y} - \mathbf{1}_M \tilde{\beta}_0^{k-1} - \mathbf{S}_{(4)}^{k-1} \tilde{\beta}_1^{k-1}\|_2^2 \end{aligned} \quad (17)$$

$$\begin{aligned} \{\tilde{\beta}_0^k, \tilde{\beta}_1^k\} = \arg \min_{\tilde{\beta}_0, \tilde{\beta}_1} \quad & \alpha \|\mathcal{P}_\Omega(\mathcal{X} - \mathcal{S}^{k-1} \times_1 \mathbf{U}_1^{k\top} \times_2 \mathbf{U}_2^{k\top} \times_3 \mathbf{U}_3^{k\top})\|_F^2 \\ & + (1 - \alpha) \|\mathbf{y} - \mathbf{1}_M \tilde{\beta}_0 - \mathbf{S}_{(4)}^{k-1} \tilde{\beta}_1\|_2^2 \end{aligned} \quad (18)$$

$$\begin{aligned} \mathcal{S}^k = \arg \min_{\mathcal{S}} \quad & \alpha \|\mathcal{P}_\Omega(\mathcal{X} - \mathcal{S} \times_1 \mathbf{U}_1^{k\top} \times_2 \mathbf{U}_2^{k\top} \times_3 \mathbf{U}_3^{k\top})\|_F^2 \\ & + (1 - \alpha) \|\mathbf{y} - \mathbf{1}_M \tilde{\beta}_0^k - \mathbf{S}_{(4)} \tilde{\beta}_1^k\|_2^2 \end{aligned} \quad (19)$$

We will discuss the analytic solutions to problems (15), (16), (17),(18), and (19) when degradation image streams are complete and incomplete in Sections 4.1 and 4.2, respectively. For simplicity, we will remove the superscripts k and $k - 1$.

4.1 Analytical Solutions for Complete Data

When degradation image streams are complete (i.e., the 4D image tensor \mathcal{X} in criterion (4) has no missing entries), we have the following Propositions 1-4, which provide the analytical solutions to problems (15), (16), (17), and (19), respectively. The solution to problem (18) is the ordinary least squares, which does not need to be discussed.

Proposition 1 *If the 4D tensor \mathcal{X} has no missing values, the optimization problem (15) has the following analytical solution*

$$\mathbf{U}_1 = (\mathbf{X}_{(1)} \cdot \mathbf{S}_{U_1(1)}^\top \cdot (\mathbf{S}_{U_1(1)} \cdot \mathbf{S}_{U_1(1)}^\top)^{-1})^\top$$

where $\mathbf{X}_{(1)}$ is the mode-1 matricization of \mathcal{X} , $\mathcal{S}_{U_1} = \mathcal{S} \times_2 \mathbf{U}_2^\top \times_3 \mathbf{U}_3^\top$, $\mathbf{S}_{U_1(1)}$ is the mode-1 matricization of \mathcal{S}_{U_1} , and the operator “ \cdot ” represents multiplication.

Proposition 2 *If the 4D tensor \mathcal{X} has no missing values, the optimization problem (16) has the following analytical solution*

$$\mathbf{U}_2 = (\mathbf{X}_{(2)} \cdot \mathbf{S}_{U_2(2)}^\top \cdot (\mathbf{S}_{U_2(2)} \cdot \mathbf{S}_{U_2(2)}^\top)^{-1})^\top$$

where $\mathbf{X}_{(2)}$ is the mode-2 matricization of \mathcal{X} , $\mathcal{S}_{U_2} = \mathcal{S} \times_1 \mathbf{U}_1^\top \times_3 \mathbf{U}_3^\top$, and $\mathbf{S}_{U_2(2)}$ is the mode-2 matricization of \mathcal{S}_{U_2} .

Proposition 3 *If the 4D tensor \mathcal{X} has no missing values, the optimization problem (17) has the following analytical solution*

$$\mathbf{U}_3 = (\mathbf{X}_{(3)} \cdot \mathbf{S}_{U_3(3)}^\top \cdot (\mathbf{S}_{U_3(3)} \cdot \mathbf{S}_{U_3(3)}^\top)^{-1})^\top$$

where $\mathbf{X}_{(3)}$ is the mode-3 matricization of \mathcal{X} , $\mathcal{S}_{U_3} = \mathcal{S} \times_1 \mathbf{U}_1^\top \times_2 \mathbf{U}_2^\top$, and $\mathbf{S}_{U_3(3)}$ is the mode-3 matricization of \mathcal{S}_{U_3} .

Proposition 4 *If the 4D tensor \mathcal{X} has no missing values, the optimization problem (19) has the following analytical solution*

$$\begin{aligned} \mathbf{S}_{(4)} &= [\alpha \cdot \mathbf{X}_{(4)} \cdot (\mathbf{U}_3 \otimes \mathbf{U}_2 \otimes \mathbf{U}_1)^\top + (1 - \alpha) \cdot (\mathbf{y} - \mathbf{1}_M \cdot \tilde{\beta}_0) \cdot \tilde{\beta}_1^\top] \cdot \\ &\quad [\alpha \cdot (\mathbf{U}_3 \otimes \mathbf{U}_2 \otimes \mathbf{U}_1) \cdot (\mathbf{U}_3 \otimes \mathbf{U}_2 \otimes \mathbf{U}_1)^\top + (1 - \alpha) \cdot \tilde{\beta}_1 \cdot \tilde{\beta}_1^\top]^{-1} \end{aligned}$$

where $\mathbf{X}_{(4)}$ is the mode-4 matricization of \mathcal{X} , $\mathbf{S}_{(4)}$ is the mode-4 matricization of \mathcal{S} .

The proof of Propositions 1-4 can be found in the Appendix.

4.2 Analytical Solutions for Incomplete Data

In this subsection, we discuss the closed-form solutions for optimization problems (15), (16), (17), (18), and (19) when the degradation tensor \mathcal{X} in criterion (4) is incomplete. We consider two data missing patterns: *entry-wise missing* and *image-wise missing*.

Entry-wise missing means that any entry of $\mathcal{X} \in \mathbb{R}^{I_1 \times I_2 \times I_3 \times M}$ can be missing. Thus, the indices of missing entries are denoted as a subset $\Omega \subseteq \{(i_1, i_2, i_3, m), 1 \leq i_1 \leq I_1, 1 \leq i_2 \leq I_2, 1 \leq i_3 \leq I_3, 1 \leq m \leq M\}$. For image-based applications, the missing elements in tensor \mathcal{X} are images but not entries, as illustrated in Figure 2(b), which yields *image-wise missing*. Thus, the subset containing the indices of missing entries can be expressed as $\Omega \subseteq \{(:, :, i_3, m), 1 \leq i_3 \leq I_3, 1 \leq m \leq M\}$, where “:” denotes all the indices in a specific dimension.

Since the solution to problem (18) is the ordinary least squares, which does not need to be discussed, we will only discuss the solutions to problems (15), (16), (17), and (19).

4.2.1 Entry-wise Missing

When the tensor \mathcal{X} has an entry-wise missing structure, there is no direct closed-form solutions for optimization criteria (15), (16), (17), and (19). However, we may decompose them into multiple sub optimization problems, each of which yields an analytical solution. To be specific, we first give the following lemma.

Lemma 1 *Let $\mathbf{A} \in \mathbb{R}^{M \times N}$, $\mathbf{C} \in \mathbb{R}^{P \times N}$, and $\mathbf{B} \in \mathbb{R}^{M \times P}$, the solution to criterion $\arg \min_{\mathbf{B}} \|\mathbf{A} - \mathbf{B}\mathbf{C}\|_F^2$ can be found by solving each row of \mathbf{B} separately—that is—solving $\{\mathbf{b}_m\}_{m=1}^M$ as follows:*

$$\arg \min_{\mathbf{b}_m} \|\mathbf{a}_m - \mathbf{b}_m \mathbf{C}\|_F^2, \quad m = 1, \dots, M$$

where $\mathbf{a}_m \in \mathbb{R}^{1 \times N}$ is the m th row of \mathbf{A} , $\mathbf{b}_m \in \mathbb{R}^{1 \times P}$ is the m th row of \mathbf{B} .

The proof of Lemma 1 can be found in the Appendix. Lemma 1 enables us to solve each column of matrices \mathbf{U}_1 , \mathbf{U}_2 , and \mathbf{U}_3 as well as each row of matrix $\mathbf{S}_{(4)}$ (the mode-4 matricization of tensor \mathcal{S}) separately.

Denote the i_1 th column of matrix $\mathbf{U}_1 \in \mathbb{R}^{P_1 \times I_1}$ as $\mathbf{u}_1^{i_1} \in \mathbb{R}^{P_1 \times 1}$, $i_1 = 1, \dots, I_1$, we replace optimization problem (15) with I_1 sub problems by separately optimizing $\mathbf{u}_1^1, \mathbf{u}_1^2, \dots, \mathbf{u}_1^{I_1}$. Proposition 5 suggests that there is an analytical solution when optimizing $\mathbf{u}_1^{i_1}$.

Proposition 5 *When optimizing the i_1 th column of \mathbf{U}_1 in Problem (15), we have the following analytical solution*

$$\mathbf{u}_1^{i_1} = (\mathbf{x}_{(1)}^{i_1, \pi_{i_1}} \cdot \mathbf{S}_{U_1(1)}^{\pi_{i_1}})^\top \cdot (\mathbf{S}_{U_1(1)}^{\pi_{i_1}} \cdot \mathbf{S}_{U_1(1)}^{\pi_{i_1} \top})^{-1})^\top$$

where $\mathbf{x}_{(1)}^{i_1}$ denotes the i_1 th row of $\mathbf{X}_{(1)}$, π_{i_1} is a set consisting of the indices of available elements of $\mathbf{x}_{(1)}^{i_1}$, $\mathbf{x}_{(1)}^{i_1, \pi_{i_1}}$ denotes a vector consisting of the available elements in the i_1 th row of $\mathbf{X}_{(1)}$, $\mathcal{S}_{U_1} = \mathcal{S} \times_2 \mathbf{U}_2^\top \times_3 \mathbf{U}_3^\top$, $\mathbf{S}_{U_1(1)}$ is the mode-1 matricization of \mathcal{S}_{U_1} , and $\mathbf{S}_{U_1(1)}^{\pi_{i_1}}$ denotes a matrix comprises the π_{i_1} columns of $\mathbf{S}_{U_1(1)}$.

Denote the i_2 th column of matrix $\mathbf{U}_2 \in \mathbb{R}^{P_2 \times I_2}$ as $\mathbf{u}_2^{i_2} \in \mathbb{R}^{P_2 \times 1}$, $i_2 = 1, \dots, I_2$, we replace optimization problem (16) with I_2 sub problems by separately optimizing $\mathbf{u}_2^1, \mathbf{u}_2^2, \dots, \mathbf{u}_2^{I_2}$. Proposition 6 suggests that there is an analytical solution when optimizing $\mathbf{u}_2^{i_2}$.

Proposition 6 *When optimizing the i_2 th column of \mathbf{U}_2 in Problem (16), we have the following analytical solution*

$$\mathbf{u}_2^{i_2} = (\mathbf{x}_{(2)}^{i_2, \pi_{i_2}} \cdot \mathbf{S}_{U_2(2)}^{\pi_{i_2}})^\top \cdot (\mathbf{S}_{U_2(2)}^{\pi_{i_2}} \cdot \mathbf{S}_{U_2(2)}^{\pi_{i_2}})^\top)^{-1}^\top$$

where $\mathbf{x}_{(2)}^{i_2}$ denotes the i_2 th row of $\mathbf{X}_{(2)}$, π_{i_2} is a set consisting of the indices of available elements of $\mathbf{x}_{(2)}^{i_2}$, $\mathbf{x}_{(2)}^{i_2, \pi_{i_2}}$ is a vector consisting of the available elements in the i_2 th column of $\mathbf{X}_{(2)}$, $\mathcal{S}_{U_2} = \mathcal{S} \times_1 \mathbf{U}_1^\top \times_3 \mathbf{U}_3^\top$, $\mathbf{S}_{U_2(2)}$ is the mode-2 matricization of \mathcal{S}_{U_2} , and $\mathbf{S}_{U_2(2)}^{\pi_{i_2}}$ denotes a matrix comprises the π_{i_2} columns of $\mathbf{S}_{U_2(2)}$.

Denote the i_3 th column of matrix $\mathbf{U}_3 \in \mathbb{R}^{P_3 \times I_3}$ as $\mathbf{u}_3^{i_3} \in \mathbb{R}^{P_3 \times 1}$, $i_3 = 1, \dots, I_3$, we replace optimization problem (17) with I_3 sub problems by separately optimizing $\mathbf{u}_3^1, \mathbf{u}_3^2, \dots, \mathbf{u}_3^{I_3}$. Proposition 7 suggests that there is an analytical solution when optimizing $\mathbf{u}_3^{i_3}$.

Proposition 7 *When optimizing the i_3 th column of \mathbf{U}_3 in Problem (17), we have the following analytical solution*

$$\mathbf{u}_3^{i_3} = (\mathbf{x}_{(3)}^{i_3, \pi_{i_3}} \cdot \mathbf{S}_{U_3(3)}^{\pi_{i_3}})^\top \cdot (\mathbf{S}_{U_3(3)}^{\pi_{i_3}} \cdot \mathbf{S}_{U_3(3)}^{\pi_{i_3}})^\top)^{-1}^\top$$

where $\mathbf{x}_{(3)}^{i_3}$ denotes the i_3 th row of $\mathbf{X}_{(3)}$, π_{i_3} is a set consisting of the indices of available elements of $\mathbf{x}_{(3)}^{i_3}$, $\mathbf{x}_{(3)}^{i_3, \pi_{i_3}}$ is a vector consisting of the available elements in the i_3 th row of $\mathbf{X}_{(3)}$, $\mathcal{S}_{U_3} = \mathcal{S} \times_1 \mathbf{U}_1^\top \times_2 \mathbf{U}_2^\top$, $\mathbf{S}_{U_3(3)}$ is the mode-3 matricization of \mathcal{S}_{U_3} , and $\mathbf{S}_{U_3(3)}^{\pi_{i_3}}$ denotes a matrix comprises the π_{i_3} columns of $\mathbf{S}_{U_3(3)}$.

Similarly, we denote the m th row of matrix $\mathbf{S}_{(4)} \in \mathbb{R}^{M \times (P_1 \times P_2 \times P_3)}$ as $\mathbf{s}_{(4)}^m \in \mathbb{R}^{1 \times (P_1 \times P_2 \times P_3)}$, $m = 1, \dots, M$, and replace optimization problem (19) with M sub problems—that is—separately optimize $\mathbf{s}_{(4)}^1, \mathbf{s}_{(4)}^2, \dots, \mathbf{s}_{(4)}^M$. Proposition 8 suggests that there is an analytical solution when optimizing $\mathbf{s}_{(4)}^m$.

Proposition 8 *When optimizing the m th row of matrix $\mathbf{S}_{(4)}$ in Problem (19), we have the following analytical solution*

$$\begin{aligned} \mathbf{s}_{(4)}^m &= [\alpha \cdot \mathbf{x}_{(4)}^{m, \pi_m} \cdot (\mathbf{U}_3 \otimes \mathbf{U}_2 \otimes \mathbf{U}_1)^{\pi_m \top} + (1 - \alpha) \cdot (y_m - \tilde{\beta}_0) \cdot \tilde{\beta}_1^\top] \cdot \\ &\quad [\alpha \cdot (\mathbf{U}_3 \otimes \mathbf{U}_2 \otimes \mathbf{U}_1)^{\pi_m} \cdot (\mathbf{U}_3 \otimes \mathbf{U}_2 \otimes \mathbf{U}_1)^{\pi_m \top} + (1 - \alpha) \cdot \tilde{\beta}_1 \cdot \tilde{\beta}_1^\top]^{-1} \end{aligned}$$

where $\mathbf{x}_{(4)}^m$ represents the m th row of $\mathbf{X}_{(4)}$, π_m denotes the set consisting of the indices of available elements in $\mathbf{x}_{(4)}^m$, $\mathbf{x}_{(4)}^{m, \pi_m}$ is a vector consisting of the available elements in the m th row of $\mathbf{X}_{(4)}$, and $(\mathbf{U}_3 \otimes \mathbf{U}_2 \otimes \mathbf{U}_1)^{\pi_m}$ denotes a matrix comprising the π_m columns of the matrix $\mathbf{U}_3 \otimes \mathbf{U}_2 \otimes \mathbf{U}_1$.

The proof of Propositions 5-8 can be found in the Appendix.

4.2.2 Image-wise Missing

When the tensor \mathcal{X} has an image-wise missing structure, Propositions 9 and 10 suggest that optimization criteria (15) and (16) have analytical solutions.

Proposition 9 *If the indices of tensor \mathcal{X} 's missing entries can be denoted as $\Omega \subseteq \{(:, :, i_3, m), 1 \leq i_3 \leq I_3, 1 \leq m \leq M\}$, where “:” denotes all the indices in a dimension, then \mathcal{X} 's mode-1 matricization $\mathbf{X}_{(1)}$ has missing columns. Let π be the set consisting of the indices of available columns in $\mathbf{X}_{(1)}$, then the optimization problem (15) has the following analytical solution*

$$\mathbf{U}_1 = (\mathbf{X}_{(1)}^\pi \cdot \mathbf{S}_{U_1(1)}^\pi \top \cdot (\mathbf{S}_{U_1(1)}^\pi \cdot \mathbf{S}_{U_1(1)}^{\pi \top})^{-1})^\top,$$

where $\mathbf{X}_{(1)}^\pi$ is a matrix consisting of the π columns of $\mathbf{X}_{(1)}$, $\mathbf{S}_{U_1} = \mathcal{S} \times_2 \mathbf{U}_2^\top \times_3 \mathbf{U}_3^\top$, $\mathbf{S}_{U_1(1)}$ is the mode-1 matricization of \mathbf{S}_{U_1} , and $\mathbf{S}_{U_1(1)}^\pi$ denotes a matrix constituting the π columns of $\mathbf{S}_{U_1(1)}$.

Proposition 10 *If the indices of tensor \mathcal{X} 's missing entries can be denoted as $\Omega \subseteq \{(:, :, i_3, m), 1 \leq i_3 \leq I_3, 1 \leq m \leq M\}$, where “:” denotes all the indices in a dimension, then \mathcal{X} 's mode-2 matricization $\mathbf{X}_{(2)}$ has missing columns. Let π be the set consisting of the indices of available columns in $\mathbf{X}_{(2)}$, then the optimization problem (16) has the following analytical solution*

$$\mathbf{U}_2 = (\mathbf{X}_{(2)}^\pi \cdot \mathbf{S}_{U_2(2)}^\pi \top \cdot (\mathbf{S}_{U_2(2)}^\pi \cdot \mathbf{S}_{U_2(2)}^{\pi \top})^{-1})^\top$$

where $\mathbf{X}_{(2)}^\pi$ is a matrix consisting of the π columns of $\mathbf{X}_{(2)}$, $\mathbf{S}_{U_2(2)}$ is the mode-2 matricization of \mathcal{S}_{U_2} , and $\mathbf{S}_{U_2(2)}^\pi$ denotes a matrix constituting the π columns of $\mathbf{S}_{U_2(2)}$.

The proof of Propositions 9-10 can be found in the Appendix.

5 Numerical Studies

In this section, we validate the effectiveness of our proposed supervised tensor dimension reduction-based prognostic model using simulated data.

5.1 Data Generation

We generate degradation image streams for 500 assets. The image stream from asset m , which is denoted by $\mathcal{X}_m(x, y, t)$, $m = 1, 2, \dots, 500$, is generated from the following heat transfer equation:

$$\frac{\partial \mathcal{X}_m(x, y, t)}{\partial t} = \alpha_m \left(\frac{\partial^2 \mathcal{X}_m}{\partial x^2} + \frac{\partial^2 \mathcal{X}_m}{\partial y^2} \right), \quad (20)$$

where $(x, y), 0 \leq x, y \leq 0.2$, represents the location of each image pixel. α_m is the thermal diffusivity coefficient, which is randomly generated from a uniform distribution $\mathcal{U}(0.5 \times 10^{-4}, 1 \times 10^{-4})$. t is the time index. The initial and boundary conditions are set such that $\mathcal{X}|_{t=1} = 0$ and $\mathcal{X}_m|_{x=0} = \mathcal{X}_m|_{x=0.2} = \mathcal{X}_m|_{y=0} = \mathcal{X}_m|_{y=0.2} = 30$. At each time t , the image is recorded at locations $x = \frac{j}{n+1}, y = \frac{k}{n+1}, j, k = 1, \dots, n$, resulting in an $n \times n$ matrix. Here, we set $n = 21$ and $t = 1, 2, \dots, 150$, which yields 150 images of size 21×21 for each asset. This implies that the degradation image stream of each asset can be represented by a $21 \times 21 \times 150$ tensor. In addition, an independent and identically distributed random noise $\epsilon \sim N(0, 0.1)$ is added to each pixel. Figure 2 demonstrates an example of some images with and without noise from one of the assets simulated in this study.

To determine the TTF of an asset, we first transform the asset's $21 \times 21 \times 150$ tensor to a 1×150 time series by taking the average pixel intensity of each image. The time series signal indicates how the average heat of the asset involves over time. Next, we let the TTF of the asset be the time point where the amplitude of the time series signal crosses a pre-defined soft failure threshold, which is set as 23 in this study. Since the images of different assets are generated with different thermal diffusivity coefficients, the time points

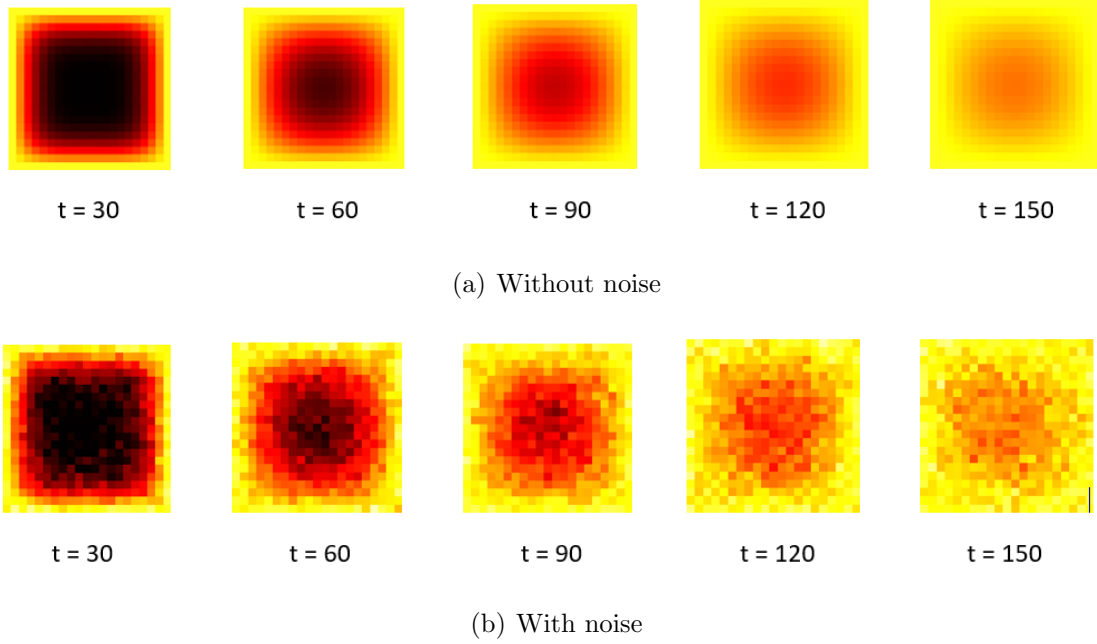


Figure 2: Simulated degradation images based on heat transfer process.

where their time series signals go beyond the threshold may be different. Thus, the TTF of different asset may also be different. To mimic reality, we truncate the image stream of each asset by keeping only the images observed before its TTF. In other words, any images observed after an asset’s TTF are removed from the image tensor of the asset. Such a truncation is normal in reality since an asset usually gets maintained or replaced once its degradation signal crosses the soft failure threshold. Consequently, the third dimension of the tensor of different assets might be different. In addition, to reduce the computation load, we keep one of every 10 images in the truncated image stream of each asset.

5.2 The Benchmark and Performance Comparison

We randomly split the generated data into a training data set consisting of 400 assets and a test data set consisting of the remaining 100 assets. To test the robustness of the proposed method, we consider four levels of data incompleteness: (1) 0% missing, (2) 10% missing, (3) 50% missing, (4) 90% missing. For the first scenario, (1) 0% missing, we use all the generated data for model training and testing. Please notice that even though all the available images are used, the image tensor \mathcal{X} is still incomplete due to failure time truncation—that is—different assets may have different TTFs and thus different number of

images (see the discussion in the second paragraph of Section 2.3). For the remaining scenarios, we randomly remove some images from each asset’s image stream. For example, when 10% missing, we randomly remove 10% of the images (rounding to the nearest integer) from the image stream of each asset.

We compare the performance of our proposed method with an unsupervised tensor dimension reduction-based benchmark. Considering image streams are incomplete, the baseline model first applies a tensor completion method known as TMac developed by Xu et al. (2013) to impute the missing values of the image tensor. Next, an unsupervised tensor dimension reduction method, MPCA (Lu et al., 2008), is employed to reduce the dimension of the imputed image tensor to reduce dimension and extract low-dimension features, which are then used to build an LLS-based prognostic model as we discussed in Section 2.3. MPCA is a widely used dimension reduction method for tensor data. It projects a high-dimensional tensor into a subspace but maximizes the total tensor scatter which is assumed to measure the variations in the original tensor objects. Lu et al. (2008) proposed a fraction-of-variation-explained (FVE) method to determine the dimension of the low-dimension tensor subspace/features, which represents the percentage of variation of the original high-dimensional tensor is preserved by the low-dimensional tensor features. Since the optimal FVE suggested by Lu et al. (2008) is 97%, we will first set FVE as 97% in this study, and the corresponding baseline model is designated as “MPCA (97%)”. In addition to the FVE method, we also use cross-validation (CV) to select an appropriate dimension for the tensor subspace. Specifically, we use the training data to conduct a 10-fold CV for various combinations of (P_1, P_2, P_3) , where $P_1 = 1, \dots, 4$, $P_2 = 1, \dots, 4$, and $P_3 = 1, \dots, 4$. The baseline model is referred to as “MPCA_CV”.

We also use 10-fold CV to determine the value of the weight parameter α and the appropriate dimension of the tensor subspace of our proposed method. Same as “MPCA_CV”, we try various combinations of (P_1, P_2, P_3) by letting P_1, P_2, P_3 vary from 1 to 4. We use the heuristic method discussed in Section 3.1 to initialize the block updating algorithm. In this study, we use lognormal regression to build the prognostic model. The proposed method is denoted as “Proposed_CV”. The prediction errors of our proposed method and two benchmarks are calculated by using the equation below and reported in Figures 3, 4, 5, and 6.

$$\text{Prediction Error} = \frac{|\text{Estimated TTF} - \text{True TTF}|}{\text{True TTF}}. \quad (21)$$

5.3 Results and analysis

Figure 3 reports the prediction errors of the two benchmarks and our proposed method when data is complete, which means no image is removed on purpose. Figure 4 shows the prediction errors when 10% elements in the 3rd mode (time) of degradation image streams are missing, while Figures 5 and 6 demonstrate the errors when 50% and 90% images are missing, respectively.

Figures 3, 4, 5, and 6 illustrate that our proposed method outperforms the benchmarks under all data missing rates. For example, when the degradation image signals are complete, the median absolute prediction errors (and the Interquartile Ranges, i.e., IQRs) of the proposed method and the two benchmarks are 0.003 (0.003), 0.027 (0.035), and 0.025 (0.033), respectively; when 10% images are missing, the median absolute prediction errors (and IQRs) of the three methods are respectively 0.019 (0.017), 0.058 (0.067), and 0.053 (0.063); when 50% of images are missing, they are 0.052 (0.084), 0.302 (0.405), and 0.104 (0.168). We believe this is because our proposed method applies historical TTFs to supervise the low-dimensional tensor dimension reduction, and thus the extracted features are more effective for failure time prediction. Unlike our method, the two baseline models use MPCA, an unsupervised tensor dimension reduction method, for feature extraction. Since the extracted features are only determined by the image streams, and no TTF gets involved, they are not as effective as the features extracted by our proposed method, and thus their failure time prediction accuracy and precision are compromised.

The figures 3, 4, 5, and 6 also suggest that the performances of all the three models deteriorate, and the superiority of our proposed method over the two benchmarks decreases, with the increase of data missing rate. For example, when data is complete, the median absolute prediction errors (and IQRs) of “Proposed_CV” and “MPCA_CV” are 0.003 (0.003) and 0.025 (0.033), respectively; when the missing rate increases to 90%, they are respectively 0.13 (0.21) and 0.16 (0.19), which are almost comparable. This is reasonable since the performance of all the models are compromised more when more data are missing. In

addition, no model will perform well if a high percentage (say more than 90%) of data are missing since it implies that very limited useful degradation information is available for modeling.

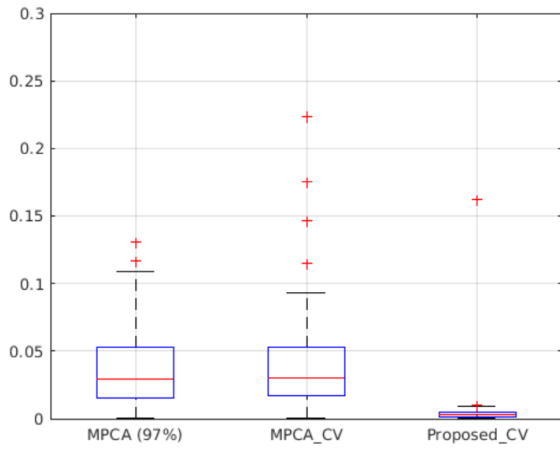


Figure 3: Prediction errors when data is complete in Numerical Study.

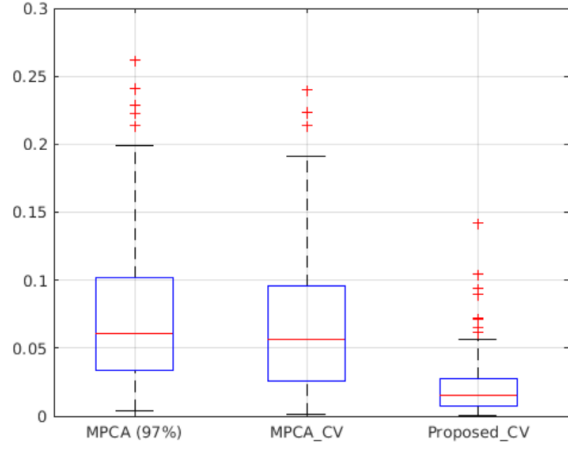


Figure 4: Prediction errors when 10% data is missing in Numerical Study.

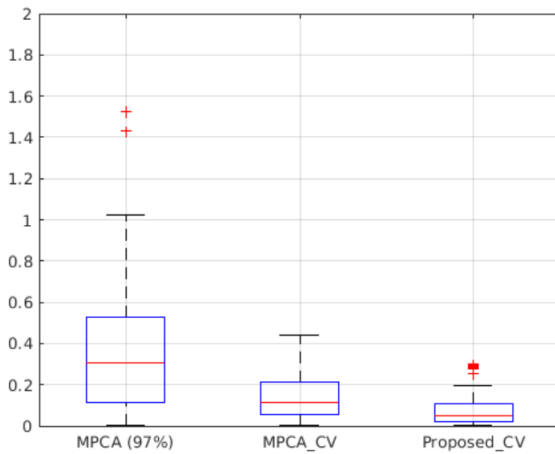


Figure 5: Prediction errors when 50% data is missing in Numerical Study.

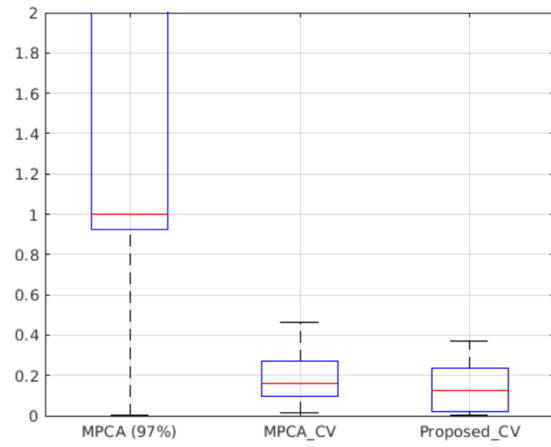


Figure 6: Prediction errors when 90% data is missing in Numerical Study.

The Figures 3-6 also demonstrate that “MPCA_CV” always outperforms “MPCA (97%)”, and the superiority of “MPCA_CV” is augmented with the increase of data missing rate. For instance, when 10% images are missing, the median absolute prediction errors (and IQR) of “MPCA (97%)” and “MPCA_CV” are 0.058 (0.067) and 0.053 (0.063), respectively; when the missing rate is 50%, they are 0.302 (0.405) and 0.104 (0.168). One of the

possible reasons is that “MPCA (97%)” determines the dimension of the tensor subspace by setting the “FVE” as 97%, which usually results in relatively high-dimensional features, although the dimension is smaller than that of the original image tensor. Relatively high-dimensional features implies an insufficient dimension reduction. In addition, it means the number of parameters in the subsequent LLS-based prognostic model is relatively large, which poses estimation challenges given that the number of samples (assets) for model training is limited.

6 Case Study

In this section, we use degradation image streams obtained from a rotating machinery test bed to validate the effectiveness of our proposed method. The test bed is designed to perform accelerated degradation tests on rolling element thrust bearings. Specifically, bearings were run from brand new to failure. An FLIR T300 infrared camera was used to monitor the degradation process and collect degradation images over time. In the meanwhile, an accelerometer was mounted on the test bed to monitor the vibration of the bearing, and the failure time is defined as the time point where the amplitude of defective vibration frequencies crosses a threshold based on ISO standards for machine vibration. The data set consists of 284 degradation image streams and their corresponding TTFs, and each image has 40×20 pixels. As an illustration, a sequence of images obtained at different (ordered) time periods of one of the bearing are shown in Figure 7. More details about the experimental setup and the data set can be found in Gebraeel et al. (2009) and Fang et al. (2019).

We use 5-fold cross validation to evaluate the performance of our proposed model and the two benchmarks discussed in Section 5. Similar to the simulation study, we conduct 10-fold cross validation to determine the optimal weight parameter in criterion (4) and the most appropriate dimension of the tensor subspace. In addition, we also consider four levels of data incompleteness: (1) 0% missing (i.e., complete), (2) 10% missing, (3) 50% missing, and (4) 90% missing. Figure 8 illustrates the absolute prediction errors when degradation image streams are complete. Figure 9 shows prediction errors when 10% of the images of each bearing are missing. Figures 10 and 11 demonstrate the absolute prediction errors

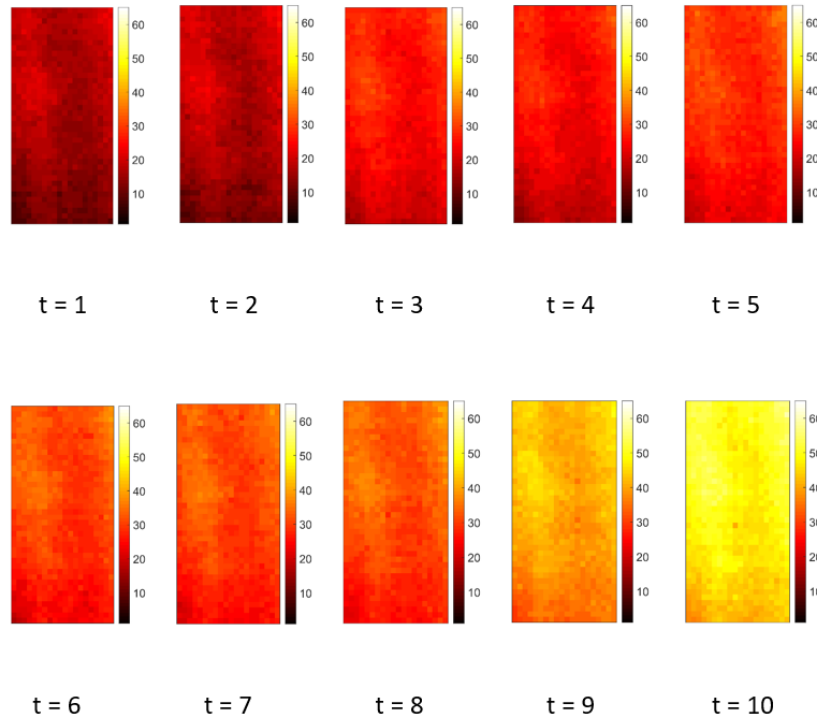


Figure 7: An illustration of one infrared degradation image stream.

when the missing rate are 50% and 90%, respectively.

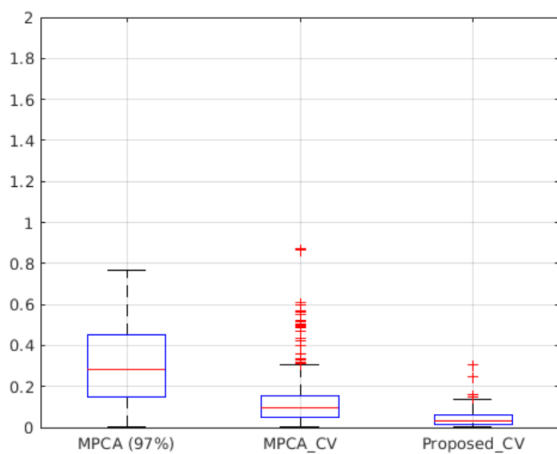


Figure 8: Prediction errors when data is complete in Case Study.

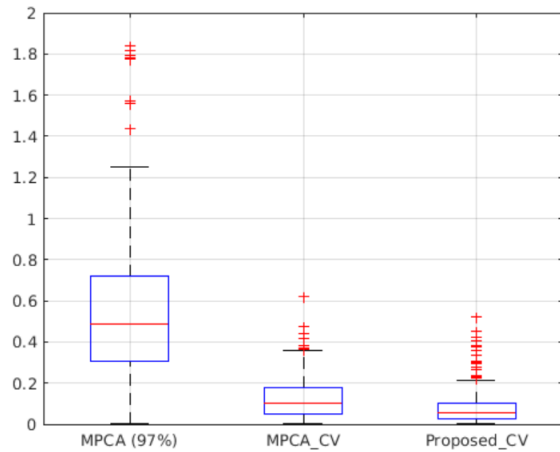


Figure 9: Prediction errors when 10% data is missing in Case Study.

Similar to the discovery in the numerical study in Section 5, Figures 8, 9, 10, and 11 indicate that our proposed method constantly works better than the two benchmarks under all the 4 data missing rates. For example, the median absolute prediction errors (and IQRs)

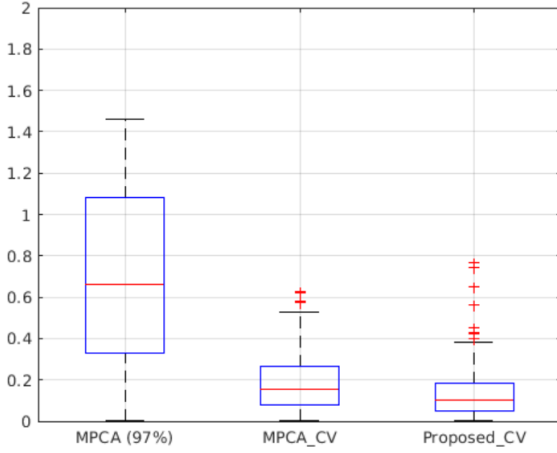


Figure 10: Prediction errors when 50% data is missing in Case Study.

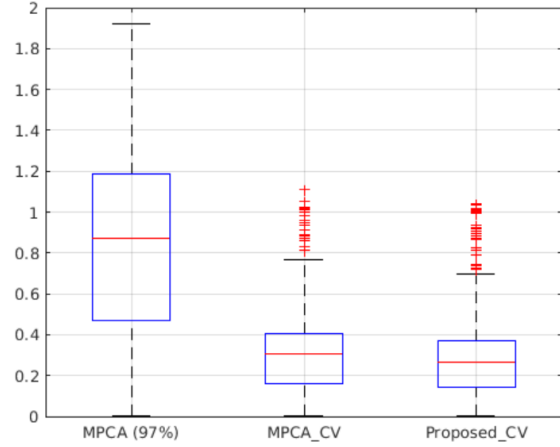


Figure 11: Prediction errors when 90% data is missing in Case Study.

of our proposed method and the two benchmarks are 0.03 (0.04), 0.3 (0.24), and 0.1 (0.16), respectively, when the degradation image streams are complete. When 50% of the images are missing, the median absolute prediction errors (and IQR) of are respectively 0.09 (0.17), 0.62 (0.65), and 0.15 (0.19). We believe this is because our proposed model is a supervised dimension reduction-based method, which uses TTF information to supervise the deflection of the low-dimensional tensor subspace, while the benchmarks are unsupervised dimension reduction-based methods without TTF information involved. Since our method considers TTF information when detecting the tensor subspace, the extracted features are more effective for failure time prediction.

Figure 8, 9, 10, 11 also show that the prediction errors of all the 3 methods increase with the increase of data missing rates. For example, when the missing rates are 0%, 10%, 50%, and 90%, the median absolute prediction errors (and IQRs) of “MPCA (97%)” are 0.3 (0.24), 0.49 (0.42), 0.62 (0.65), and 0.83 (0.78), respectively, while they are respectively 0.09 (0.11), 0.1 (0.16), 0.15 (0.19), and 0.31 (0.22) for “MPCA_CV”, and 0.03 (0.04), 0.05 (0.08), 0.09 (0.17), and 0.29 (0.21) for our proposed method. This is reasonable since a higher data missing rate means less useful degradation information and thus a worse model performance. In addition, we observe that the superiority of our proposed method over the two benchmarks decrease with the increase of data missing rates. For example, the prediction accuracy of our method and “MPCA (97%)” are comparable when the data

missing rate is 90%. We again believe this is because not much useful information is available when data is highly incomplete and none of the two models perform well with such limited data.

We also observe that “MPCA_CV” always outperforms “MPCA (97%)”, and the superiority of “MPCA_CV” is augmented with the increase of data missing rate. For example, when 10% images are missing, the median absolute prediction errors (and IQR) of “MPCA (97%)” and MPCA_CV are 0.49 (0.42) and 0.1 (0.16), respectively; when the missing rate is 50%, they are 0.62 (0.65) and 0.15 (0.19). We again believe this is because “MPCA (97%)” determines the dimension of the tensor subspace by setting the “FVE” as 97%, which results in relatively high-dimensional features due to the insufficient dimension reduction. Also, it results in a parameter estimation challenge since the number of parameters to be estimated in the prognostic model is relatively large comparing to the limited number of historical samples for model training. This suggests that cross validation is a better method to determine the dimension of the tensor subspace, especially when we do not have enough number of samples for model training.

7 Conclusions

This paper proposed a supervised tensor dimension reduction-based prognostic model for applications with incomplete degradation imaging data. This is achieved by first developing a new supervised tensor dimension reduction method that reduces the dimension of incomplete high-dimensional degradation image streams and provides low-dimensional tensor features, which are then used to build a prognostic model based on (log)-location-scale regression.

The supervised tensor dimension reduction method uses historical TTFs to supervise the detection of a low-dimensional tensor subspace to reduce the dimension of incomplete high-dimensional image streams. Mathematically, it is formulated as an optimization criterion that combines a feature extraction term and a regression term. The feature extraction term focuses on identifying a tensor space to extract low-dimensional tensor features from high-dimensional image streams. The regression term regresses failure times against the features extracted by the first term using LLS regression. By jointly optimizing the two terms, it

is expected to detect an appropriate tensor subspace such that the extracted features are effective for TTF prediction. To estimate the parameters of the supervised dimension reduction method, we developed a Block Updating Algorithm for applications where TTFs follow distributions in the (log)-location-scale family. The algorithm works by splitting the parameters into several blocks and cyclically optimizing one block of parameters while keeping other blocks fixed until convergence. In addition, we showed that if TTFs follow normal or lognormal distributions, there is a closed form solution when optimizing each block of the parameters, no matter the imaging data is complete or incomplete.

Simulated data as well as a data set from rotating machinery were used to validate the effectiveness of our proposed method. The results showed that our proposed prognostic method consistently outperforms the unsupervised tensor reduction-based benchmarks under various data missing rates. This validated the benefits and importance of using failure time information to supervise the dimension reduction of high-dimensional degradation image streams when building prognostic models.

Appendix

1 Proof of Proposition 1

The original optimization problem is

$$\arg \min_{\mathbf{U}_1} \alpha \|\mathcal{P}_\Omega(\mathcal{X} - \mathcal{S} \times_1 \mathbf{U}_1^\top \times_2 \mathbf{U}_2^\top \times_3 \mathbf{U}_3^\top)\|_F^2 + (1 - \alpha) \|\mathbf{y} - \mathbf{1}_M \cdot \tilde{\beta}_0 - \mathcal{S}_{(4)} \cdot \tilde{\beta}_1\|_F^2,$$

which is equivalent to the following problem when data is complete:

$$\arg \min_{\mathbf{U}_1} \alpha \|\mathcal{X} - \mathcal{S} \times_1 \mathbf{U}_1^\top \times_2 \mathbf{U}_2^\top \times_3 \mathbf{U}_3^\top\|_F^2 + (1 - \alpha) \|\mathbf{y} - \mathbf{1}_M \cdot \tilde{\beta}_0 - \mathcal{S}_{(4)} \cdot \tilde{\beta}_1\|_F^2,$$

which is convex. Thus, it can be solved by setting the derivatives to be zeros—that is $\frac{d\Psi}{d\mathbf{U}_1} = \mathbf{0}$, where $\Psi = \alpha \|\mathcal{X} - \mathcal{S} \times_1 \mathbf{U}_1^\top \times_2 \mathbf{U}_2^\top \times_3 \mathbf{U}_3^\top\|_F^2 + (1 - \alpha) \|\mathbf{y} - \mathbf{1}_M \cdot \tilde{\beta}_0 - \mathcal{S}_{(4)} \cdot \tilde{\beta}_1\|_F^2$. This implies $\frac{d}{d\mathbf{U}_1} (\|\mathcal{X} - \mathcal{S} \times_1 \mathbf{U}_1^\top \times_2 \mathbf{U}_2^\top \times_3 \mathbf{U}_3^\top\|_F^2) = \mathbf{0}$. According to the communication law of tensor mode multiplication, we have $\frac{d}{d\mathbf{U}_1} (\|\mathcal{X} - (\mathcal{S} \times_2 \mathbf{U}_2^\top \times_3 \mathbf{U}_3^\top) \times_1 \mathbf{U}_1^\top\|_F^2) = \mathbf{0}$. Thus, $\frac{d}{d\mathbf{U}_1} (\|\mathcal{X} - \mathcal{S}_{\mathbf{U}_1} \times_1 \mathbf{U}_1^\top\|_F^2) = \mathbf{0}$, where $\mathcal{S}_{\mathbf{U}_1} = \mathcal{S} \times_2 \mathbf{U}_2^\top \times_3 \mathbf{U}_3^\top$. Furthermore, we have $\frac{d}{d\mathbf{U}_1} (\|\mathbf{X}_{(1)} - \mathbf{U}_1^\top \cdot \mathcal{S}_{\mathbf{U}_1(1)}\|_F^2) = \mathbf{0}$ due to the fact that $\|\mathcal{S}\|_F^2 = \|\mathcal{S}_{(n)}\|_F^2$ and the property of tensor mode multiplication $\mathcal{S} \times_n \mathbf{U} = \mathbf{U} \cdot \mathcal{S}_{(n)}$. By taking the derivative of the Frobenius norm, we have $2(\mathbf{X}_{(1)} - \mathbf{U}_1^\top \cdot \mathcal{S}_{\mathbf{U}_1(1)}) \cdot (-\mathcal{S}_{\mathbf{U}_1(1)}^\top) = \mathbf{0}$. Thus, $\mathbf{U}_1^\top \cdot \mathcal{S}_{\mathbf{U}_1(1)} \cdot \mathcal{S}_{\mathbf{U}_1(1)}^\top = \mathbf{X}_{(1)} \cdot \mathcal{S}_{\mathbf{U}_1(1)}^\top$, which gives that $\mathbf{U}_1^\top = \mathbf{X}_{(1)} \cdot \mathcal{S}_{\mathbf{U}_1(1)}^\top \cdot (\mathcal{S}_{\mathbf{U}_1(1)} \cdot \mathcal{S}_{\mathbf{U}_1(1)}^\top)^{-1}$. Finally, we have $\mathbf{U}_1 = (\mathbf{X}_{(1)} \cdot \mathcal{S}_{\mathbf{U}_1(1)}^\top \cdot (\mathcal{S}_{\mathbf{U}_1(1)} \cdot \mathcal{S}_{\mathbf{U}_1(1)}^\top)^{-1})^\top$.

2 Proof of Proposition 2

The original optimization problem is

$$\arg \min_{\mathbf{U}_2} \alpha \|\mathcal{P}_\Omega(\mathcal{X} - \mathcal{S} \times_1 \mathbf{U}_1^\top \times_2 \mathbf{U}_2^\top \times_3 \mathbf{U}_3^\top)\|_F^2 + (1 - \alpha) \|\mathbf{y} - \mathbf{1}_M \cdot \tilde{\beta}_0 - \mathcal{S}_{(4)} \cdot \tilde{\beta}_1\|_F^2,$$

which is equivalent to the following problem when data is complete:

$$\arg \min_{\mathbf{U}_2} \alpha \|\mathcal{X} - \mathcal{S} \times_1 \mathbf{U}_1^\top \times_2 \mathbf{U}_2^\top \times_3 \mathbf{U}_3^\top\|_F^2 + (1 - \alpha) \|\mathbf{y} - \mathbf{1}_M \cdot \tilde{\beta}_0 - \mathcal{S}_{(4)} \cdot \tilde{\beta}_1\|_F^2$$

which is convex. Therefore, it can be solved by setting the derivatives to be zeros—that is $\frac{d\Psi}{d\mathbf{U}_2} = \mathbf{0}$, where $\Psi = \alpha \|\mathcal{X} - \mathcal{S} \times_1 \mathbf{U}_1^\top \times_2 \mathbf{U}_2^\top \times_3 \mathbf{U}_3^\top\|_F^2 + (1 - \alpha) \|\mathbf{y} - \mathbf{1}_M \cdot \tilde{\beta}_0 - \mathcal{S}_{(4)} \cdot \tilde{\beta}_1\|_F^2$.

This implies $\frac{d}{d\mathbf{U}_2}(\|\mathcal{X} - \mathcal{S} \times_1 \mathbf{U}_1^\top \times_2 \mathbf{U}_2^\top \times_3 \mathbf{U}_3^\top\|_F^2) = \mathbf{0}$. According to the communication law of tensor mode multiplication, we have $\frac{d}{d\mathbf{U}_2}(\|\mathcal{X} - (\mathcal{S} \times_1 \mathbf{U}_1^\top \times_3 \mathbf{U}_3^\top) \times_2 \mathbf{U}_2^\top\|_F^2) = \mathbf{0}$. Thus, $\frac{d}{d\mathbf{U}_2}(\|\mathcal{X} - \mathcal{S}_{U_2} \times_2 \mathbf{U}_2^\top\|_F^2) = \mathbf{0}$, where $\mathcal{S}_{U_2} = \mathcal{S} \times_1 \mathbf{U}_1^\top \times_3 \mathbf{U}_3^\top$. Furthermore, we have $\frac{d}{d\mathbf{U}_2}(\|\mathbf{X}_{(2)} - \mathbf{U}_2^\top \cdot \mathbf{S}_{U_2(2)}\|_F^2) = \mathbf{0}$ due to the fact that $\|\mathcal{S}\|_F^2 = \|\mathbf{S}_{(n)}\|_F^2$ and the property of tensor mode multiplication $\mathcal{S} \times_n \mathbf{U} = \mathbf{U} \cdot \mathbf{S}_{(n)}$. By taking the derivative of the Frobenius norm, we have $2(\mathbf{X}_{(2)} - \mathbf{U}_2^\top \cdot \mathbf{S}_{U_2(2)}) \cdot (-\mathbf{S}_{U_2(2)}^\top) = \mathbf{0}$. Thus, $\mathbf{U}_2^\top \cdot \mathbf{S}_{U_2(2)} \cdot \mathbf{S}_{U_2(2)}^\top = \mathbf{X}_{(2)} \cdot \mathbf{S}_{U_2(2)}^\top$ which gives that $\mathbf{U}_2^\top = \mathbf{X}_{(2)} \cdot \mathbf{S}_{U_2(2)}^\top \cdot (\mathbf{S}_{U_2(2)} \cdot \mathbf{S}_{U_2(2)}^\top)^{-1}$. Finally we have $\mathbf{U}_2 = (\mathbf{X}_{(2)} \cdot \mathbf{S}_{U_2(2)}^\top \cdot (\mathbf{S}_{U_2(2)} \cdot \mathbf{S}_{U_2(2)}^\top)^{-1})^\top$.

3 Proof of Proposition 3

The original optimization problem is

$$\arg \min_{\mathbf{U}_3} \alpha \|\mathcal{P}_\Omega(\mathcal{X} - \mathcal{S} \times_1 \mathbf{U}_1^\top \times_2 \mathbf{U}_2^\top \times_3 \mathbf{U}_3^\top)\|_F^2 + (1 - \alpha) \|\mathbf{y} - \mathbf{1}_M \cdot \tilde{\beta}_0 - \mathbf{S}_{(4)} \cdot \tilde{\beta}_1\|_F^2,$$

which is equivalent to the following problem when data is complete:

$$\arg \min_{\mathbf{U}_3} \alpha \|\mathcal{X} - \mathcal{S} \times_1 \mathbf{U}_1^\top \times_2 \mathbf{U}_2^\top \times_3 \mathbf{U}_3^\top\|_F^2 + (1 - \alpha) \|\mathbf{y} - \mathbf{1}_M \cdot \tilde{\beta}_0 - \mathbf{S}_{(4)} \cdot \tilde{\beta}_1\|_F^2$$

which is convex. Therefore, it can be solved by setting the derivatives to be zeros—that is $\frac{d\Psi}{d\mathbf{U}_3} = \mathbf{0}$, where $\Psi = \alpha \|\mathcal{X} - \mathcal{S} \times_1 \mathbf{U}_1^\top \times_2 \mathbf{U}_2^\top \times_3 \mathbf{U}_3^\top\|_F^2 + (1 - \alpha) \|\mathbf{y} - \mathbf{1}_M \cdot \tilde{\beta}_0 - \mathbf{S}_{(4)} \cdot \tilde{\beta}_1\|_F^2$. This implies $\frac{d}{d\mathbf{U}_3}(\|\mathcal{X} - \mathcal{S} \times_1 \mathbf{U}_1^\top \times_2 \mathbf{U}_2^\top \times_3 \mathbf{U}_3^\top\|_F^2) = \mathbf{0}$. According to the communication law of tensor mode multiplication, we have $\frac{d}{d\mathbf{U}_3}(\|\mathcal{X} - (\mathcal{S} \times_1 \mathbf{U}_1^\top \times_2 \mathbf{U}_2^\top) \times_3 \mathbf{U}_3^\top\|_F^2) = \mathbf{0}$. Thus, $\frac{d}{d\mathbf{U}_3}(\|\mathcal{X} - \mathcal{S}_{U_3} \times_3 \mathbf{U}_3^\top\|_F^2) = \mathbf{0}$, where $\mathcal{S}_{U_3} = \mathcal{S} \times_1 \mathbf{U}_1^\top \times_2 \mathbf{U}_2^\top$. Furthermore, we have $\frac{d}{d\mathbf{U}_3}(\|\mathbf{X}_{(3)} - \mathbf{U}_3^\top \cdot \mathbf{S}_{U_3(3)}\|_F^2) = \mathbf{0}$ due to the fact that $\|\mathcal{S}\|_F^2 = \|\mathbf{S}_{(n)}\|_F^2$ and the property of tensor mode multiplication $\mathcal{S} \times_n \mathbf{U} = \mathbf{U} \cdot \mathbf{S}_{(n)}$. By taking the derivative of the Frobenius norm, we have $2(\mathbf{X}_{(3)} - \mathbf{U}_3^\top \cdot \mathbf{S}_{U_3(3)}) \cdot (-\mathbf{S}_{U_3(3)}^\top) = \mathbf{0}$. Thus, $\mathbf{U}_3^\top \cdot \mathbf{S}_{U_3(3)} \cdot \mathbf{S}_{U_3(3)}^\top = \mathbf{X}_{(3)} \cdot \mathbf{S}_{U_3(3)}^\top$, which gives that $\mathbf{U}_3^\top = \mathbf{X}_{(3)} \cdot \mathbf{S}_{U_3(3)}^\top \cdot (\mathbf{S}_{U_3(3)} \cdot \mathbf{S}_{U_3(3)}^\top)^{-1}$. Finally, we have $\mathbf{U}_3 = (\mathbf{X}_{(3)} \cdot \mathbf{S}_{U_3(3)}^\top \cdot (\mathbf{S}_{U_3(3)} \cdot \mathbf{S}_{U_3(3)}^\top)^{-1})^\top$.

4 Proof of Proposition 4

The original optimization problem is

$$\arg \min_{\mathbf{S}} \alpha \|\mathcal{P}_\Omega(\mathcal{X} - \mathcal{S} \times_1 \mathbf{U}_1^\top \times_2 \mathbf{U}_2^\top \times_3 \mathbf{U}_3^\top)\|_F^2 + (1 - \alpha) \|\mathbf{y} - \mathbf{1}_M \cdot \tilde{\beta}_0 - \mathbf{S}_{(4)} \cdot \tilde{\beta}_1\|_F^2,$$

which is equivalent to the following problem when data is complete:

$$\arg \min_{\hat{\mathcal{S}}} \alpha \|\mathcal{X} - \mathcal{S} \times_1 \mathbf{U}_1^\top \times_2 \mathbf{U}_2^\top \times_3 \mathbf{U}_3^\top\|_F^2 + (1 - \alpha) \|\mathbf{y} - \mathbf{1}_M \cdot \tilde{\beta}_0 - \mathcal{S}_{(4)} \cdot \tilde{\beta}_1\|_F^2,$$

which is convex. Thus, it can be solved by setting the derivatives to be zeros—that is $\frac{d\Psi}{d\mathcal{S}} = \mathbf{0}$, where $\Psi = \alpha \|\mathcal{X} - \mathcal{S} \times_1 \mathbf{U}_1^\top \times_2 \mathbf{U}_2^\top \times_3 \mathbf{U}_3^\top\|_F^2 + (1 - \alpha) \|\mathbf{y} - \mathbf{1}_M \cdot \tilde{\beta}_0 - \mathcal{S}_{(4)} \cdot \tilde{\beta}_1\|_F^2$. According to the connection between Kronecker product and tensor mode multiplication (Kolda, 2006), we have $\frac{d}{d\mathcal{S}}(\alpha \|\mathbf{X}_{(4)} - \mathcal{S}_{(4)} \cdot (\mathbf{U}_3 \otimes \mathbf{U}_2 \otimes \mathbf{U}_1)\|_F^2 + (1 - \alpha) \|\mathbf{y} - \mathbf{1}_M \cdot \tilde{\beta}_0 - \mathcal{S}_{(4)} \cdot \tilde{\beta}_1\|_F^2) = \mathbf{0}$. By taking the derivative of the Frobenius norm, we have $2\alpha \cdot [\mathbf{X}_{(4)} - \mathcal{S}_{(4)} \cdot (\mathbf{U}_3 \otimes \mathbf{U}_2 \otimes \mathbf{U}_1)] \cdot [-(\mathbf{U}_3 \otimes \mathbf{U}_2 \otimes \mathbf{U}_1)^\top] + 2(1 - \alpha) \cdot [\mathbf{y} - \mathbf{1}_M \cdot \tilde{\beta}_0 - \mathcal{S}_{(4)} \cdot \tilde{\beta}_1] \cdot (-\tilde{\beta}_1^\top) = \mathbf{0}$. Thus, $-2\alpha \cdot \mathbf{X}_{(4)} \cdot (\mathbf{U}_3 \otimes \mathbf{U}_2 \otimes \mathbf{U}_1)^\top + 2\alpha \cdot \mathcal{S}_{(4)} \cdot (\mathbf{U}_3 \otimes \mathbf{U}_2 \otimes \mathbf{U}_1) \cdot (\mathbf{U}_3 \otimes \mathbf{U}_2 \otimes \mathbf{U}_1)^\top + 2(1 - \alpha)(\mathbf{y} - \mathbf{1}_M \cdot \tilde{\beta}_0) \cdot (-\tilde{\beta}_1^\top) + 2(1 - \alpha) \cdot (\mathcal{S}_{(4)} \cdot \tilde{\beta}_1 \cdot \tilde{\beta}_1^\top) = \mathbf{0}$. Finally, we have $\mathcal{S}_{(4)} = [\alpha \cdot \mathbf{X}_{(4)} \cdot (\mathbf{U}_3 \otimes \mathbf{U}_2 \otimes \mathbf{U}_1)^\top + (1 - \alpha) \cdot (\mathbf{y} - \mathbf{1}_M \cdot \tilde{\beta}_0) \cdot \tilde{\beta}_1^\top] \cdot [\alpha \cdot (\mathbf{U}_3 \otimes \mathbf{U}_2 \otimes \mathbf{U}_1) \cdot (\mathbf{U}_3 \otimes \mathbf{U}_2 \otimes \mathbf{U}_1)^\top + (1 - \alpha) \cdot \tilde{\beta}_1 \cdot \tilde{\beta}_1^\top]^{-1}$.

5 Proof of Lemma 1

Let $\mathbf{a}_m \in \mathbb{R}^{1 \times N}$ denotes the m th row of matrix $\mathbf{A} \in \mathbb{R}^{M \times N}$ and $\mathbf{b}_m \in \mathbb{R}^{1 \times P}$ denotes the m th row of matrix $\mathbf{B} \in \mathbb{R}^{M \times P}$, $m = 1, \dots, M$, then we have

$$\mathbf{A} - \mathbf{BC} = [(\mathbf{a}_1 - \mathbf{b}_1\mathbf{C})^\top, \dots, (\mathbf{a}_M - \mathbf{b}_M\mathbf{C})^\top]^\top.$$

Based on the definition of Frobenius norm, the original objective function in Lemma 1 can be transformed as follows:

$$\|\mathbf{A} - \mathbf{BC}\|_F^2 = \|[(\mathbf{a}_1 - \mathbf{b}_1\mathbf{C})^\top, \dots, (\mathbf{a}_M - \mathbf{b}_M\mathbf{C})^\top]^\top\|_F^2 = \sum_{m=1}^M \|\mathbf{a}_m - \mathbf{b}_m\mathbf{C}\|_F^2.$$

Therefore, we have the following:

$$\arg \min_{\mathbf{B}} \|\mathbf{A} - \mathbf{BC}\|_F^2 = \arg \min_{\{\mathbf{b}_m\}_{m=1}^M} \sum_{m=1}^M \|\mathbf{a}_m - \mathbf{b}_m\mathbf{C}\|_F^2.$$

where $\mathbf{B} = [\mathbf{b}_1^\top, \dots, \mathbf{b}_M^\top]^\top$. Therefore, to solve the original objective function, we can simply solve the following M sub problems:

$$\arg \min_{\mathbf{b}_m} \|\mathbf{a}_m - \mathbf{b}_m\mathbf{C}\|_F^2, \quad m = 1, \dots, M.$$

6 Proof of Proposition 5

The original optimization problem is

$$\arg \min_{\mathbf{U}_1} \alpha \|\mathcal{P}_\Omega(\mathcal{X} - \mathcal{S} \times_1 \mathbf{U}_1^\top \times_2 \mathbf{U}_2^\top \times_3 \mathbf{U}_3^\top)\|_F^2 + (1 - \alpha) \|\mathbf{y} - \mathbf{1}_M \cdot \tilde{\beta}_0 - \mathcal{S}_{(4)} \cdot \tilde{\beta}_1\|_F^2,$$

which is equivalent to the following problem when data is missing:

$$\arg \min_{\mathbf{U}_1} \alpha \|\mathcal{X} - (\mathcal{S} \times_1 \mathbf{U}_1^\top \times_2 \mathbf{U}_2^\top \times_3 \mathbf{U}_3^\top) \odot \text{logic}(\mathcal{X})\|_F^2 + (1 - \alpha) \|\mathbf{y} - \mathbf{1}_M \cdot \tilde{\beta}_0 - \mathcal{S}_{(4)} \cdot \tilde{\beta}_1\|_F^2,$$

where \odot is the inner product, $\text{logic}(\mathcal{X})$ denotes the logical value of \mathcal{X} —that is—if an entry is observed, its logical value is 1; otherwise, it is 0. Since the problem is convex, it can be solved by setting the derivatives to be zeros, i.e., $\frac{d\Psi}{d\mathbf{U}_1} = \mathbf{0}$, where $\Psi = \alpha \|\mathcal{X} - (\mathcal{S} \times_1 \mathbf{U}_1^\top \times_2 \mathbf{U}_2^\top \times_3 \mathbf{U}_3^\top) \odot \text{logic}(\mathcal{X})\|_F^2 + (1 - \alpha) \|\mathbf{y} - \mathbf{1}_M \cdot \tilde{\beta}_0 - \mathcal{S}_{(4)} \cdot \tilde{\beta}_1\|_F^2$. This implies $\frac{d}{d\mathbf{U}_1} (\|\mathcal{X} - (\mathcal{S} \times_1 \mathbf{U}_1^\top \times_2 \mathbf{U}_2^\top \times_3 \mathbf{U}_3^\top) \odot \text{logic}(\mathcal{X})\|_F^2) = \mathbf{0}$. According to the communication law of tensor mode multiplication, we have $\frac{d}{d\mathbf{U}_1} (\|\mathcal{X} - [(\mathcal{S} \times_1 \mathbf{U}_1^\top \times_2 \mathbf{U}_2^\top) \times_3 \mathbf{U}_3^\top] \odot \text{logic}(\mathcal{X})\|_F^2) = \mathbf{0}$. Thus, $\frac{d}{d\mathbf{U}_1} (\|\mathcal{X} - (\mathcal{S}_{U_1} \times_1 \mathbf{U}_1^\top) \odot \text{logic}(\mathcal{X})\|_F^2) = \mathbf{0}$, where $\mathcal{S}_{U_1} = \mathcal{S} \times_2 \mathbf{U}_2^\top \times_3 \mathbf{U}_3^\top$. Furthermore, we have $\frac{d}{d\mathbf{U}_1} (\|\mathbf{X}_{(1)} - (\mathbf{U}_1^\top \cdot \mathcal{S}_{U_1(1)}) \odot \text{logic}(\mathbf{X}_{(1)})\|_F^2) = \mathbf{0}$ since $\|\mathcal{S}\|_F^2 = \|\mathcal{S}_{(n)}\|_F^2$ and $\mathcal{S} \times_n \mathbf{U} = \mathbf{U} \cdot \mathcal{S}_{(n)}$.

Figure 12 shows the pattern of mode-1 matricization of the 4D tensor \mathcal{X} when it has missing entries whose indices can be denoted by a set $\Omega \subseteq \{(i_1, i_2, i_3, m), 1 \leq i_1 \leq I_1, 1 \leq i_2 \leq I_2, 1 \leq i_3 \leq I_3, 1 \leq m \leq M\}$. Based on Lemma 1, we can sequentially optimize each column of \mathbf{U}_1 .

Specifically, we denote the i_1 th row in \mathbf{U}_1^\top as $\mathbf{u}_1^{i_1\top}$ (blue solid row of \mathbf{U}_1^\top in Figure 12). The available elements in the i_1 th row of $\mathbf{X}_{(1)}$ are denoted as $\mathbf{x}_{(1)}^{i_1, \pi_{i_1}}$ (blue striped squares of $\mathbf{x}_{(1)}^{i_1}$ in Figure 12). In $\mathcal{S}_{U_1(1)}^{\pi_{i_1}}$, we choose the columns whose indices are the same as those of the available elements of $\mathbf{x}_{(1)}^{i_1}$ (blue striped columns of $\mathcal{S}_{U_1(1)}^{\pi_{i_1}}$ in Figure 12). As a result, we have $\frac{d}{d\mathbf{u}_1^{i_1}} (\sum_{i_1=1}^{I_1} \|\mathbf{x}_{(1)}^{i_1, \pi_{i_1}} - (\mathbf{u}_1^{i_1\top} \cdot \mathcal{S}_{U_1(1)}^{\pi_{i_1}})\|_F^2) = \mathbf{0}$. Because we only take the derivative of $\mathbf{u}_1^{i_1}$, we have $\frac{d}{d\mathbf{u}_1^{i_1}} (\|\mathbf{x}_{(1)}^{i_1, \pi_{i_1}} - (\mathbf{u}_1^{i_1\top} \cdot \mathcal{S}_{U_1(1)}^{\pi_{i_1}})\|_F^2) = \mathbf{0}$. By taking the derivative of the Frobenius norm, we have $2(\mathbf{x}_{(1)}^{i_1, \pi_{i_1}} - \mathbf{u}_1^{i_1\top} \cdot \mathcal{S}_{U_1(1)}^{\pi_{i_1}}) \cdot (-\mathcal{S}_{U_1(1)}^{\pi_{i_1}\top}) = \mathbf{0}$. Thus, $\mathbf{u}_1^{i_1\top} \cdot \mathcal{S}_{U_1(1)}^{\pi_{i_1}} \cdot \mathcal{S}_{U_1(1)}^{\pi_{i_1}\top} = \mathbf{x}_{(1)}^{i_1, \pi_{i_1}} \cdot \mathcal{S}_{U_1(1)}^{\pi_{i_1}\top}$, which gives that $\mathbf{u}_1^{i_1} = (\mathbf{x}_{(1)}^{i_1, \pi_{i_1}} \cdot \mathcal{S}_{U_1(1)}^{\pi_{i_1}\top} \cdot (\mathcal{S}_{U_1(1)}^{\pi_{i_1}} \cdot \mathcal{S}_{U_1(1)}^{\pi_{i_1}\top})^{-1})^\top$.

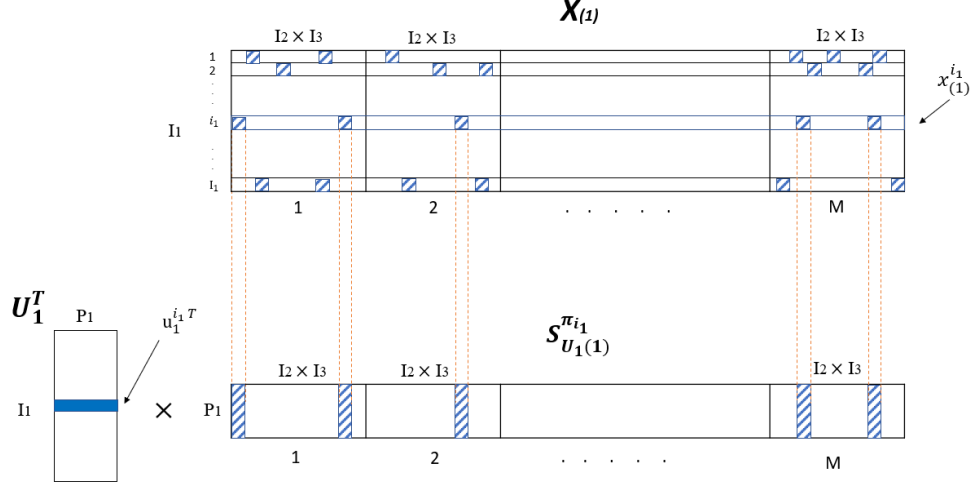


Figure 12: An illustration of the data missing pattern in Proposition 5 (stripes representing available elements).

7 Proof of Proposition 6

The original optimization problem is

$$\arg \min_{\mathbf{U}_2} \alpha \|\mathcal{P}_\Omega(\mathcal{X} - \mathcal{S} \times_1 \mathbf{U}_1^\top \times_2 \mathbf{U}_2^\top \times_3 \mathbf{U}_3^\top)\|_F^2 + (1 - \alpha) \|\mathbf{y} - \mathbf{1}_M \cdot \tilde{\beta}_0 - \mathcal{S}_{(4)} \cdot \tilde{\beta}_1\|_F^2,$$

which is equivalent to the following problem when data is missing:

$$\arg \min_{\mathbf{U}_2} \alpha \|\mathcal{X} - (\mathcal{S} \times_1 \mathbf{U}_1^\top \times_2 \mathbf{U}_2^\top \times_3 \mathbf{U}_3^\top) \odot \text{logic}(\mathcal{X})\|_F^2 + (1 - \alpha) \|\mathbf{y} - \mathbf{1}_M \cdot \tilde{\beta}_0 - \mathcal{S}_{(4)} \cdot \tilde{\beta}_1\|_F^2,$$

where \odot is the inner product, $\text{logic}(\mathcal{X})$ denotes the logical value of \mathcal{X} . Since the problem is convex, it can be solved by setting the derivatives to be zeros, i.e., $\frac{d\Psi}{d\mathbf{U}_2} = \mathbf{0}$, where $\Psi = \alpha \|\mathcal{X} - (\mathcal{S} \times_1 \mathbf{U}_1^\top \times_2 \mathbf{U}_2^\top \times_3 \mathbf{U}_3^\top) \odot \text{logic}(\mathcal{X})\|_F^2 + (1 - \alpha) \|\mathbf{y} - \mathbf{1}_M \cdot \tilde{\beta}_0 - \mathcal{S}_{(4)} \cdot \tilde{\beta}_1\|_F^2$. This implies $\frac{d}{d\mathbf{U}_2} (\|\mathcal{X} - (\mathcal{S} \times_1 \mathbf{U}_1^\top \times_2 \mathbf{U}_2^\top \times_3 \mathbf{U}_3^\top) \odot \text{logic}(\mathcal{X})\|_F^2) = \mathbf{0}$. According to the communication law of tensor mode multiplication, we have $\frac{d}{d\mathbf{U}_2} (\|\mathcal{X} - [(\mathcal{S} \times_1 \mathbf{U}_1^\top \times_3 \mathbf{U}_3^\top) \times_2 \mathbf{U}_2^\top] \odot \text{logic}(\mathcal{X})\|_F^2) = \mathbf{0}$. Thus, $\frac{d}{d\mathbf{U}_2} (\|\mathcal{X} - (\mathcal{S}_{U_2} \times_2 \mathbf{U}_2^\top) \odot \text{logic}(\mathcal{X})\|_F^2) = \mathbf{0}$, where $\mathcal{S}_{U_2} = \mathcal{S} \times_1 \mathbf{U}_1^\top \times_3 \mathbf{U}_3^\top$. Furthermore, we have $\frac{d}{d\mathbf{U}_2} (\|\mathbf{X}_{(2)} - (\mathbf{U}_2^\top \cdot \mathcal{S}_{U_2(2)}) \odot \text{logic}(\mathbf{X}_{(2)})\|_F^2) = \mathbf{0}$ since $\|\mathcal{S}\|_F^2 = \|\mathcal{S}_{(n)}\|_F^2$ and $\mathcal{S} \times_n \mathbf{U} = \mathbf{U} \cdot \mathcal{S}_{(n)}$.

Figure 13 shows the pattern of mode-2 matricization of the 4D tensor \mathcal{X} when it has missing entries whose indices can be denoted by a set $\Omega \subseteq \{(i_1, i_2, i_3, m), 1 \leq i_1 \leq I_1, 1 \leq i_2 \leq I_2, 1 \leq i_3 \leq I_3, 1 \leq m \leq M\}$. Based on Lemma 1, we can sequentially optimize each column of \mathbf{U}_2 .

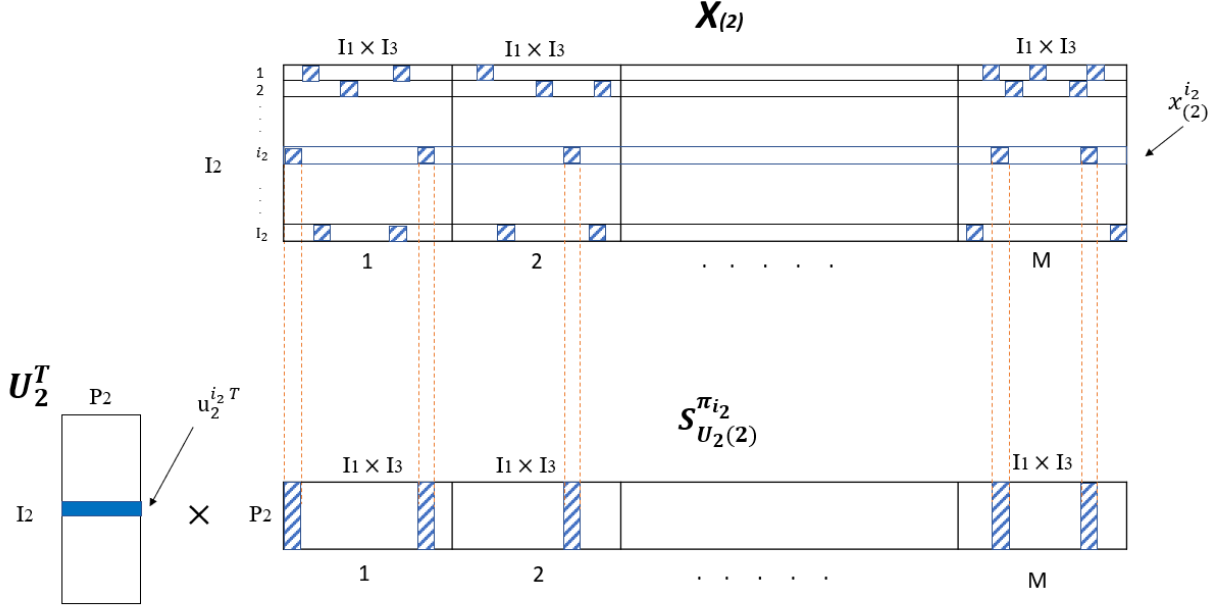


Figure 13: An illustration of the data missing pattern in Proposition 6 (stripes representing available elements).

Specifically, we denote the i_2 th row in \mathbf{U}_2^\top as $\mathbf{u}_2^{i_2^\top}$ (blue solid row of \mathbf{U}_2^\top in Figure 13). The available elements in the i_2 th row of $\mathbf{X}_{(2)}$ are denoted as $\mathbf{x}_{(2)}^{i_2, \pi_{i_2}}$ (blue striped squares of $\mathbf{x}_{(2)}^{i_2}$ in Figure 13). In $\mathbf{S}_{U_2(2)}^{\pi_{i_2}}$, we choose the columns whose indices are the same as those of the available elements in $\mathbf{x}_{(2)}^{i_2}$ (blue striped columns of $\mathbf{S}_{U_2(2)}^{\pi_{i_2}}$ in Figure 13). As a result, we have $\frac{d}{d\mathbf{u}_2^{i_2}} (\sum_{i_2=1}^{I_2} \|\mathbf{x}_{(2)}^{i_2, \pi_{i_2}} - (\mathbf{u}_2^{i_2^\top} \cdot \mathbf{S}_{U_2(2)}^{\pi_{i_2}})\|_F^2) = \mathbf{0}$. Since on the derivative of $\mathbf{u}_2^{i_2}$ is taken, we have $\frac{d}{d\mathbf{u}_2^{i_2}} (\|\mathbf{x}_{(2)}^{i_2, \pi_{i_2}} - (\mathbf{u}_2^{i_2^\top} \cdot \mathbf{S}_{U_2(2)}^{\pi_{i_2}})\|_F^2) = \mathbf{0}$. By taking the derivative of the Frobenius norm, we have $2(\mathbf{x}_{(2)}^{i_2, \pi_{i_2}} - \mathbf{u}_2^{i_2^\top} \cdot \mathbf{S}_{U_2(2)}^{\pi_{i_2}}) \cdot (-\mathbf{S}_{U_2(2)}^{\pi_{i_2}^\top}) = \mathbf{0}$. Thus, $\mathbf{u}_2^{i_2^\top} \cdot \mathbf{S}_{U_2(2)}^{\pi_{i_2}} \cdot \mathbf{S}_{U_2(2)}^{\pi_{i_2}^\top} = \mathbf{x}_{(2)}^{i_2, \pi_{i_2}} \cdot \mathbf{S}_{U_2(2)}^{\pi_{i_2}^\top}$, which gives that $\mathbf{u}_2^{i_2} = (\mathbf{x}_{(2)}^{i_2, \pi_{i_2}} \cdot \mathbf{S}_{U_2(2)}^{\pi_{i_2}^\top} \cdot (\mathbf{S}_{U_2(2)}^{\pi_{i_2}} \cdot \mathbf{S}_{U_2(2)}^{\pi_{i_2}^\top})^{-1})^\top$.

8 Proof of Proposition 7

The original optimization problem is

$$\arg \min_{\mathbf{U}_3} \alpha \|\mathcal{P}_\Omega(\mathcal{X} - \mathcal{S} \times_1 \mathbf{U}_1^\top \times_2 \mathbf{U}_2^\top \times_3 \mathbf{U}_3^\top)\|_F^2 + (1 - \alpha) \|\mathbf{y} - \mathbf{1}_M \cdot \tilde{\beta}_0 - \mathcal{S}_{(4)} \cdot \tilde{\beta}_1\|_F^2,$$

which is equivalent to the following problem when data is missing:

$$\arg \min_{\mathbf{U}_3} \alpha \|\mathcal{X} - (\mathcal{S} \times_1 \mathbf{U}_1^\top \times_2 \mathbf{U}_2^\top \times_3 \mathbf{U}_3^\top) \odot \text{logic}(\mathcal{X})\|_F^2 + (1 - \alpha) \|\mathbf{y} - \mathbf{1}_M \cdot \tilde{\beta}_0 - \mathcal{S}_{(4)} \cdot \tilde{\beta}_1\|_F^2,$$

where \odot is the inner product, $\text{logic}(\mathcal{X})$ denotes the logical value of \mathcal{X} . Since the problem is convex, it can be solved by setting the derivatives to be zeros, i.e., $\frac{d\Psi}{d\mathbf{U}_3} = \mathbf{0}$, where $\Psi = \alpha \|\mathcal{X} - (\mathcal{S} \times_1 \mathbf{U}_1^\top \times_2 \mathbf{U}_2^\top \times_3 \mathbf{U}_3^\top) \odot \text{logic}(\mathcal{X})\|_F^2 + (1 - \alpha) \|\mathbf{y} - \mathbf{1}_M \cdot \tilde{\beta}_0 - \mathcal{S}_{(4)} \cdot \tilde{\beta}_1\|_F^2$. This implies $\frac{d}{d\mathbf{U}_3} (\|\mathcal{X} - (\mathcal{S} \times_1 \mathbf{U}_1^\top \times_2 \mathbf{U}_2^\top \times_3 \mathbf{U}_3^\top) \odot \text{logic}(\mathcal{X})\|_F^2) = \mathbf{0}$. According to the communication law of tensor mode multiplication, we have $\frac{d}{d\mathbf{U}_3} (\|\mathcal{X} - [(\mathcal{S} \times_1 \mathbf{U}_1^\top \times_2 \mathbf{U}_2^\top) \times_3 \mathbf{U}_3^\top] \odot \text{logic}(\mathcal{X})\|_F^2) = \mathbf{0}$. Thus, $\frac{d}{d\mathbf{U}_3} (\|\mathcal{X} - (\mathcal{S}_{U_3} \times_3 \mathbf{U}_3^\top) \odot \text{logic}(\mathcal{X})\|_F^2) = \mathbf{0}$, where $\mathcal{S}_{U_3} = \mathcal{S} \times_1 \mathbf{U}_1^\top \times_2 \mathbf{U}_2^\top$. Furthermore, we have $\frac{d}{d\mathbf{U}_3} (\|\mathbf{X}_{(3)} - (\mathbf{U}_3^\top \cdot \mathcal{S}_{U_3(3)}) \odot \text{logic}(\mathbf{X}_{(3)})\|_F^2) = \mathbf{0}$ since $\|\mathcal{S}\|_F^2 = \|\mathcal{S}_{(n)}\|_F^2$ and $\mathcal{S} \times_n \mathbf{U} = \mathbf{U} \cdot \mathcal{S}_{(n)}$.

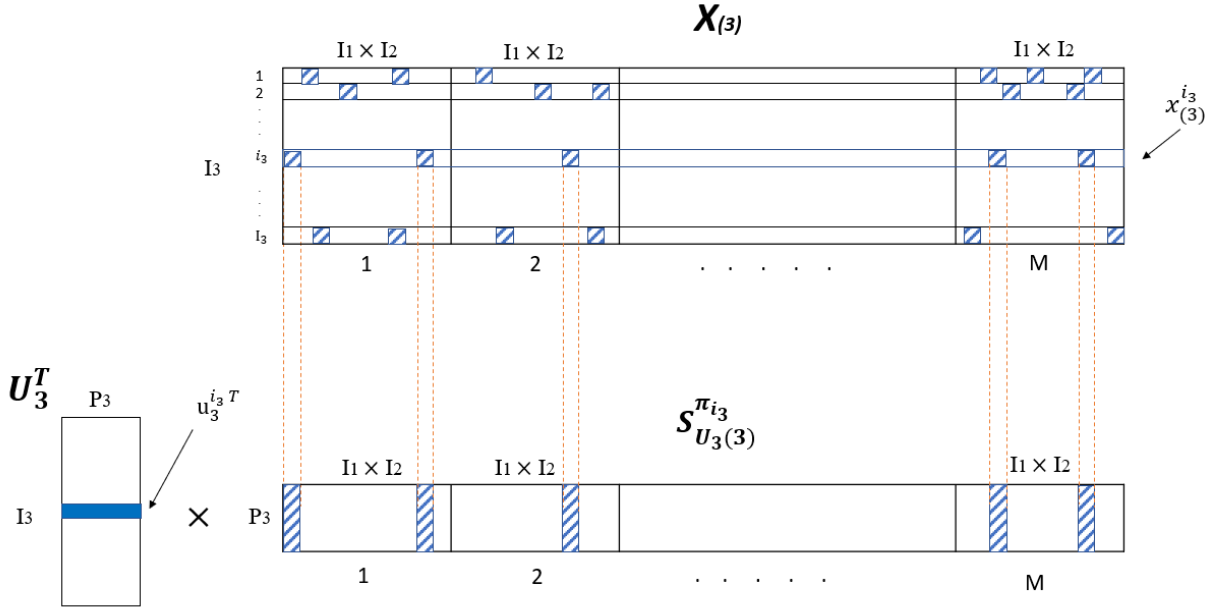


Figure 14: An illustration of the data missing pattern in Proposition 7 (stripes representing available elements).

Figure 14 shows the pattern of mode-3 matricization of the 4D tensor \mathcal{X} when it has missing entries whose indices can be denoted by a set $\Omega \subseteq \{(i_1, i_2, i_3, m), 1 \leq i_1 \leq I_1, 1 \leq i_2 \leq I_2, 1 \leq i_3 \leq I_3, 1 \leq m \leq M\}$. Based on Lemma 1, we can sequentially optimize each column of \mathbf{U}_3 . The i_3 th row in \mathbf{U}_3^\top is denoted as $\mathbf{u}_3^{i_3 \top}$ (blue solid row of \mathbf{U}_3^\top in Figure 14). The available elements in the i_3 th row of $\mathbf{X}_{(3)}$ are denoted as $\mathbf{x}_{(3)}^{i_3, \pi_{i_3}}$ (blue striped squares of $\mathbf{x}_{(3)}^{i_3}$ in Figure 14). In $\mathcal{S}_{U_3(3)}^{\pi_{i_3}}$, we choose the columns whose indices are the same as those of the available elements of $\mathbf{x}_{(3)}^{i_3}$ (blue striped columns of $\mathcal{S}_{U_3(3)}^{\pi_{i_3}}$ in Figure 14). Thus, we have $\frac{d}{d\mathbf{u}_3^{i_3 \top}} (\sum_{i_3=1}^{I_3} \|\mathbf{x}_{(3)}^{i_3, \pi_{i_3}} - (\mathbf{u}_3^{i_3 \top} \cdot \mathcal{S}_{U_3(3)}^{\pi_{i_3}})\|_F^2) = \mathbf{0}$, which yields

$\frac{d}{d\mathbf{u}_3^{i_3}}(\|\mathbf{x}_{(3)}^{i_3, \pi_{i_3}} - (\mathbf{u}_3^{i_3 \top} \cdot \mathbf{S}_{U_3(3)}^{\pi_{i_3}})\|_F^2) = \mathbf{0}$. By taking the derivative of the Frobenius norm, we have $2(\mathbf{x}_{(3)}^{i_3, \pi_{i_3}} - \mathbf{u}_3^{i_3 \top} \cdot \mathbf{S}_{U_3(3)}^{\pi_{i_3}}) \cdot (-\mathbf{S}_{U_3(3)}^{\pi_{i_3} \top}) = \mathbf{0}$. Thus, $\mathbf{u}_3^{i_3 \top} \cdot \mathbf{S}_{U_3(3)}^{\pi_{i_3}} \cdot \mathbf{S}_{U_3(3)}^{\pi_{i_3} \top} = \mathbf{x}_{(3)}^{i_3, \pi_{i_3}} \cdot \mathbf{S}_{U_3(3)}^{\pi_{i_3} \top}$, which gives that $\mathbf{u}_3^{i_3} = (\mathbf{x}_{(3)}^{i_3, \pi_{i_3}} \cdot \mathbf{S}_{U_3(3)}^{\pi_{i_3} \top} \cdot (\mathbf{S}_{U_3(3)}^{\pi_{i_3}} \cdot \mathbf{S}_{U_3(3)}^{\pi_{i_3} \top})^{-1})^\top$.

9 Proof of Proposition 8

The original optimization problem is

$$\arg \min_{\mathcal{S}} \alpha \|\mathcal{P}_\Omega(\mathcal{X} - \mathcal{S} \times_1 \mathbf{U}_1^\top \times_2 \mathbf{U}_2^\top \times_3 \mathbf{U}_3^\top)\|_F^2 + (1 - \alpha) \|\mathbf{y} - \mathbf{1}_M \cdot \tilde{\beta}_0 - \mathbf{S}_{(4)} \cdot \tilde{\beta}_1\|_F^2$$

which is equivalent to the following problem when data is missing:

$$\arg \min_{\mathcal{S}} \alpha \|\mathcal{X} - (\mathcal{S} \times_1 \mathbf{U}_1^\top \times_2 \mathbf{U}_2^\top \times_3 \mathbf{U}_3^\top) \odot \text{logic}(\mathcal{X})\|_F^2 + (1 - \alpha) \|\mathbf{y} - \mathbf{1}_M \cdot \tilde{\beta}_0 - \mathbf{S}_{(4)} \cdot \tilde{\beta}_1\|_F^2$$

where \odot is the inner product, $\text{logic}(\mathcal{X})$ denotes the logical value of \mathcal{X} . Since the problem is convex, it can be solved by setting the derivative to be zeros—that is $\frac{d\Psi}{d\mathcal{S}} = \mathbf{0}$, where $\Psi = \alpha \|\mathcal{X} - (\mathcal{S} \times_1 \mathbf{U}_1^\top \times_2 \mathbf{U}_2^\top \times_3 \mathbf{U}_3^\top) \odot \text{logic}(\mathcal{X})\|_F^2 + (1 - \alpha) \|\mathbf{y} - \mathbf{1}_M \cdot \tilde{\beta}_0 - \mathbf{S}_{(4)} \cdot \tilde{\beta}_1\|_F^2$. According to the connection between Kronecker product and tensor mode multiplication, we have $\frac{d}{d\mathcal{S}}(\alpha \|\mathbf{X}_{(4)} - [\mathbf{S}_{(4)} \cdot (\mathbf{U}_3 \otimes \mathbf{U}_2 \otimes \mathbf{U}_1)] \odot \text{logic}(\mathbf{X}_{(4)})\|_F^2 + (1 - \alpha) \|\mathbf{y} - \mathbf{1}_M \odot \tilde{\beta}_0 - \mathbf{S}_{(4)} \odot \tilde{\beta}_1\|_F^2) = \mathbf{0}$.

Figure 15 shows the pattern of mode-4 matricization of the 4D tensor \mathcal{X} when it has missing entries whose indices can be denoted by a set $\Omega \subseteq \{(i_1, i_2, i_3, m), 1 \leq i_1 \leq I_1, 1 \leq i_2 \leq I_2, 1 \leq i_3 \leq I_3, 1 \leq m \leq M\}$. Based on Lemma 1, we can sequentially optimize each column of \mathbf{U}_3 .

The m th row in $\mathbf{S}_{(4)}$ is denoted as $\mathbf{s}_{(4)}^m$ (blue solid row of $\mathbf{S}_{(4)}$ in Figure 15). The available elements in the m th row of $\mathbf{X}_{(4)}$ are denoted as $\mathbf{x}_{(4)}^{m, \pi_m}$ (blue striped squares of $\mathbf{x}_{(4)}^m$ in Figure 15). In $(\mathbf{U}_3 \otimes \mathbf{U}_2 \otimes \mathbf{U}_1)$, we choose the columns whose indices are the same as those of the available elements of $\mathbf{x}_{(4)}^m$ (blue striped columns of $(\mathbf{U}_3 \otimes \mathbf{U}_2 \otimes \mathbf{U}_1)^{\pi_m}$ in Figure 15). Thus, we have $\frac{d}{d\mathbf{s}_{(4)}^m}(\alpha \{\sum_{m=1}^M \|\mathbf{x}_{(4)}^{m, \pi_m} - [\mathbf{s}_{(4)}^m \cdot (\mathbf{U}_3 \otimes \mathbf{U}_2 \otimes \mathbf{U}_1)^{\pi_m}]\|_F^2 + (1 - \alpha) \sum_{m=1}^M \|y_m - \tilde{\beta}_0 - \mathbf{s}_{(4)}^m \cdot \tilde{\beta}_1\|_F^2) = \mathbf{0}$, which yields $\frac{d}{d\mathbf{s}_{(4)}^m}(\alpha \{\|\mathbf{x}_{(4)}^{m, \pi_m} - [\mathbf{s}_{(4)}^m \cdot (\mathbf{U}_3 \otimes \mathbf{U}_2 \otimes \mathbf{U}_1)^{\pi_m}]\|_F^2 + (1 - \alpha) \|y_m - \tilde{\beta}_0 - \mathbf{s}_{(4)}^m \cdot \tilde{\beta}_1\|_F^2) = \mathbf{0}$. By taking the derivative of Frobenius norm, we have $2\alpha \cdot [\mathbf{x}_{(4)}^{m, \pi_m} - \mathbf{s}_{(4)}^m] \cdot (\mathbf{U}_3 \otimes \mathbf{U}_2 \otimes \mathbf{U}_1)^{\pi_m} \cdot [-(\mathbf{U}_3 \otimes \mathbf{U}_2 \otimes \mathbf{U}_1)^{\pi_m \top}] + 2(1 - \alpha) \cdot [y_m - \tilde{\beta}_0 - \mathbf{s}_{(4)}^m \cdot \tilde{\beta}_1] \cdot (-\tilde{\beta}_1^\top) = \mathbf{0}$. Thus, $-2\alpha \cdot \mathbf{x}_{(4)}^{m, \pi_m} \cdot (\mathbf{U}_3 \otimes \mathbf{U}_2 \otimes \mathbf{U}_1)^{\pi_m \top} + 2\alpha \cdot \mathbf{s}_{(4)}^m \cdot (\mathbf{U}_3 \otimes \mathbf{U}_2 \otimes \mathbf{U}_1)^{\pi_m} \cdot (\mathbf{U}_3 \otimes \mathbf{U}_2 \otimes \mathbf{U}_1)^{\pi_m \top} + 2(1 - \alpha)(y_m - \tilde{\beta}_0) \cdot (-\tilde{\beta}_1^\top) + 2(1 - \alpha) \cdot (\mathbf{s}_{(4)}^m \cdot \tilde{\beta}_1 \cdot \tilde{\beta}_1^\top) = \mathbf{0}$, which gives that $\mathbf{s}_{(4)}^m = [\alpha \cdot \mathbf{x}_{(4)}^{m, \pi_m} \cdot (\mathbf{U}_3 \otimes \mathbf{U}_2 \otimes \mathbf{U}_1)^{\pi_m \top} + (1 - \alpha) \cdot (y_m - \tilde{\beta}_0) \cdot \tilde{\beta}_1^\top] \cdot [\alpha \cdot (\mathbf{U}_3 \otimes \mathbf{U}_2 \otimes \mathbf{U}_1)^{\pi_m} \cdot (\mathbf{U}_3 \otimes \mathbf{U}_2 \otimes \mathbf{U}_1)^{\pi_m \top} + (1 - \alpha) \cdot \tilde{\beta}_1 \cdot \tilde{\beta}_1^\top]^{-1}$.

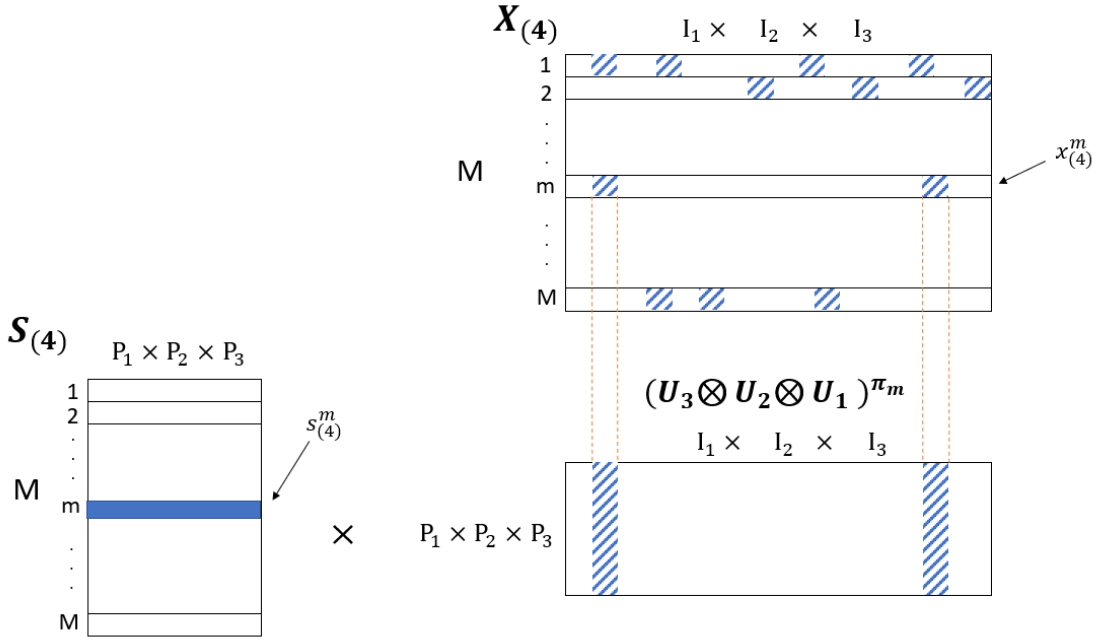


Figure 15: An illustration of the data missing pattern in Proposition 8 (stripes representing available elements).

10 Proof of Proposition 9

The original optimization problem is

$$\arg \min_{\mathbf{U}_1} \alpha \|\mathcal{P}_\Omega(\mathcal{X} - \mathcal{S} \times_1 \mathbf{U}_1^\top \times_2 \mathbf{U}_2^\top \times_3 \mathbf{U}_3^\top)\|_F^2 + (1 - \alpha) \|\mathbf{y} - \mathbf{1}_M \cdot \tilde{\beta}_0 - \mathcal{S}_{(4)} \cdot \tilde{\beta}_1\|_F^2,$$

which is equivalent to the following problem when data is incomplete:

$$\arg \min_{\mathbf{U}_1} \alpha \|\mathcal{X} - (\mathcal{S} \times_1 \mathbf{U}_1^\top \times_2 \mathbf{U}_2^\top \times_3 \mathbf{U}_3^\top) \odot \text{logic}(\mathcal{X})\|_F^2 + (1 - \alpha) \|\mathbf{y} - \mathbf{1}_M \cdot \tilde{\beta}_0 - \mathcal{S}_{(4)} \cdot \tilde{\beta}_1\|_F^2,$$

where \odot is the inner product, $\text{logic}(\mathcal{X})$ denotes the logical value of \mathcal{X} . Since the problem is convex, it can be solved by setting the derivatives to be zeros, i.e., $\frac{d\Psi}{d\mathbf{U}_1} = \mathbf{0}$, where $\Psi = \alpha \|\mathcal{X} - (\mathcal{S} \times_1 \mathbf{U}_1^\top \times_2 \mathbf{U}_2^\top \times_3 \mathbf{U}_3^\top) \odot \text{logic}(\mathcal{X})\|_F^2 + (1 - \alpha) \|\mathbf{y} - \mathbf{1}_M \cdot \tilde{\beta}_0 - \mathcal{S}_{(4)} \cdot \tilde{\beta}_1\|_F^2$. This implies $\frac{d}{d\mathbf{U}_1} (\|\mathcal{X} - (\mathcal{S} \times_1 \mathbf{U}_1^\top \times_2 \mathbf{U}_2^\top \times_3 \mathbf{U}_3^\top) \odot \text{logic}(\mathcal{X})\|_F^2) = \mathbf{0}$. According to the communication law of tensor mode multiplication, we have $\frac{d}{d\mathbf{U}_1} (\|\mathcal{X} - [(\mathcal{S} \times_2 \mathbf{U}_2^\top \times_3 \mathbf{U}_3^\top) \times_1 \mathbf{U}_1^\top] \odot \text{logic}(\mathcal{X})\|_F^2) = \mathbf{0}$. Thus, $\frac{d}{d\mathbf{U}_1} (\|\mathcal{X} - (\mathcal{S}_{U_1} \times_1 \mathbf{U}_1^\top) \odot \text{logic}(\mathcal{X})\|_F^2) = \mathbf{0}$, where $\mathcal{S}_{U_1} = \mathcal{S} \times_2 \mathbf{U}_2^\top \times_3 \mathbf{U}_3^\top$. Furthermore, we have $\frac{d}{d\mathbf{U}_1} (\|\mathbf{X}_{(1)} - (\mathbf{U}_1^\top \cdot \mathcal{S}_{U_1(1)}) \odot \text{logic}(\mathbf{X}_{(1)})\|_F^2) = \mathbf{0}$ due to the fact that $\|\mathcal{S}\|_F^2 = \|\mathcal{S}_{(n)}\|_F^2$ and $\mathcal{S} \times_n \mathbf{U} = \mathbf{U} \cdot \mathcal{S}_{(n)}$ (a property of tensor mode multiplication).

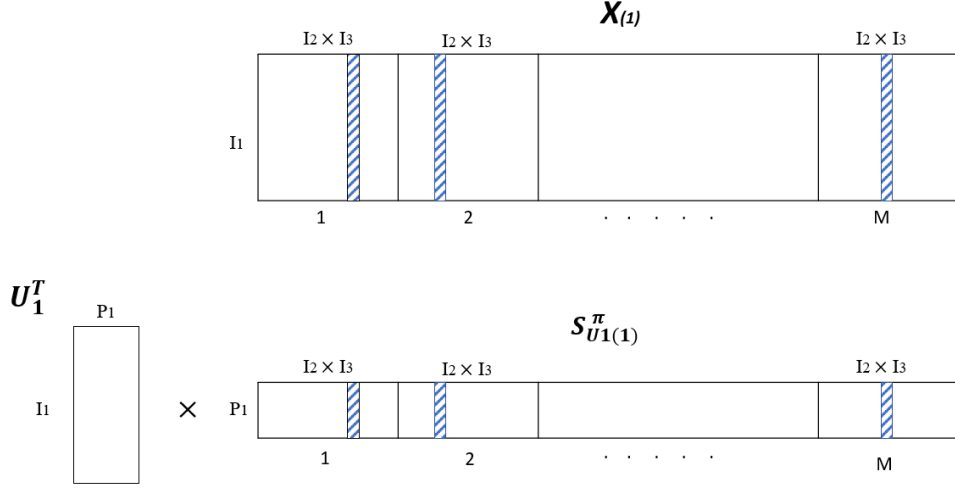


Figure 16: An illustration of the data missing pattern in Proposition 9 (stripes representing available columns).

As discussed earlier, for applications with missing images, the indices of tensor \mathcal{X} 's missing entries can be denoted as $\Omega \subseteq \{(:, :, i_3, m), 1 \leq i_3 \leq I_3, 1 \leq m \leq M\}$, where “:” denotes all the indices in a dimension. As a result, it can be easily shown that \mathcal{X} 's mode-1 matricization $\mathbf{X}_{(1)}$ has missing columns (see Figure 16 for an illustration). Let π be the set consisting of the indices of available columns in $\mathbf{X}_{(1)}$, then we need to solve $\frac{d}{d\mathbf{U}_1} (\|\mathbf{X}_{(1)}^\pi - \mathbf{U}_1^\top \cdot \mathbf{S}_{U_1(1)}^\pi\|_F^2) = \mathbf{0}$, where $\mathbf{S}_{U_1(1)}^\pi$ denotes a matrix constituting the π columns of $\mathbf{S}_{U_1(1)}$. Thus, we have $2(\mathbf{X}_{(1)}^\pi - \mathbf{U}_1^\top \cdot \mathbf{S}_{U_1(1)}^\pi) \cdot (-\mathbf{S}_{U_1(1)}^{\pi \top}) = \mathbf{0}$. Thus, $\mathbf{U}_1^\top \cdot \mathbf{S}_{U_1(1)}^\pi \cdot \mathbf{S}_{U_1(1)}^{\pi \top} = \mathbf{X}_{(1)}^\pi \cdot \mathbf{S}_{U_1(1)}^{\pi \top}$, which gives that $\mathbf{U}_1^\top = \mathbf{X}_{(1)}^\pi \cdot \mathbf{S}_{U_1(1)}^{\pi \top} \cdot (\mathbf{S}_{U_1(1)}^\pi \cdot \mathbf{S}_{U_1(1)}^{\pi \top})^{-1}$. This yields the solution $\mathbf{U}_1 = (\mathbf{X}_{(1)}^\pi \cdot \mathbf{S}_{U_1(1)}^{\pi \top} \cdot (\mathbf{S}_{U_1(1)}^\pi \cdot \mathbf{S}_{U_1(1)}^{\pi \top})^{-1})^\top$.

11 Proof of Proposition 10

The original optimization problem is

$$\arg \min_{\mathbf{U}_2} \alpha \|\mathcal{P}_\Omega(\mathcal{X} - \mathcal{S} \times_1 \mathbf{U}_1^\top \times_2 \mathbf{U}_2^\top \times_3 \mathbf{U}_3^\top)\|_F^2 + (1 - \alpha) \|\mathbf{y} - \mathbf{1}_M \cdot \tilde{\beta}_0 - \mathbf{S}_{(4)} \cdot \tilde{\beta}_1\|_F^2,$$

which is equivalent to the following problem when data is incomplete:

$$\arg \min_{\mathbf{U}_2} \alpha \|\mathcal{X} - (\mathcal{S} \times_1 \mathbf{U}_1^\top \times_2 \mathbf{U}_2^\top \times_3 \mathbf{U}_3^\top) \odot \text{logic}(\mathcal{X})\|_F^2 + (1 - \alpha) \|\mathbf{y} - \mathbf{1}_M \cdot \tilde{\beta}_0 - \mathbf{S}_{(4)} \cdot \tilde{\beta}_1\|_F^2,$$

where \odot is the inner product, $\text{logic}(\mathcal{X})$ denotes the logical value of \mathcal{X} . Since the optimization criterion is convex, it can be solved by setting the derivatives to be zeros, i.e., $\frac{d\Psi}{d\mathbf{U}_2} = \mathbf{0}$, where $\Psi = \alpha \|\mathcal{X} - (\mathcal{S} \times_1 \mathbf{U}_1^\top \times_2 \mathbf{U}_2^\top \times_3 \mathbf{U}_3^\top) \odot \text{logic}(\mathcal{X})\|_F^2 + (1 - \alpha) \|\mathbf{y} - \mathbf{1}_M \cdot \tilde{\beta}_0 - \mathcal{S}_{(4)} \cdot \tilde{\beta}_1\|_F^2$. This implies $\frac{d}{d\mathbf{U}_2} (\|\mathcal{X} - (\mathcal{S} \times_1 \mathbf{U}_1^\top \times_2 \mathbf{U}_2^\top \times_3 \mathbf{U}_3^\top) \odot \text{logic}(\mathcal{X})\|_F^2) = \mathbf{0}$. According to the communication law of tensor mode multiplication, we have $\frac{d}{d\mathbf{U}_2} (\|\mathcal{X} - [(\mathcal{S} \times_1 \mathbf{U}_1^\top \times_3 \mathbf{U}_3^\top) \times_2 \mathbf{U}_2^\top] \odot \text{logic}(\mathcal{X})\|_F^2) = \mathbf{0}$. As a result, $\frac{d}{d\mathbf{U}_2} (\|\mathcal{X} - (\mathcal{S}_{U_2} \times_2 \mathbf{U}_2^\top) \odot \text{logic}(\mathcal{X})\|_F^2) = \mathbf{0}$, where $\mathcal{S}_{U_2} = \mathcal{S} \times_1 \mathbf{U}_1^\top \times_3 \mathbf{U}_3^\top$. Furthermore, we have $\frac{d}{d\mathbf{U}_2} (\|\mathbf{X}_{(2)} - (\mathbf{U}_2^\top \cdot \mathbf{S}_{U_2(2)}) \odot \text{logic}(\mathbf{X}_{(2)})\|_F^2) = \mathbf{0}$ since $\|\mathcal{S}\|_F^2 = \|\mathbf{S}_{(n)}\|_F^2$ and $\mathcal{S} \times_n \mathbf{U} = \mathbf{U} \cdot \mathbf{S}_{(n)}$.

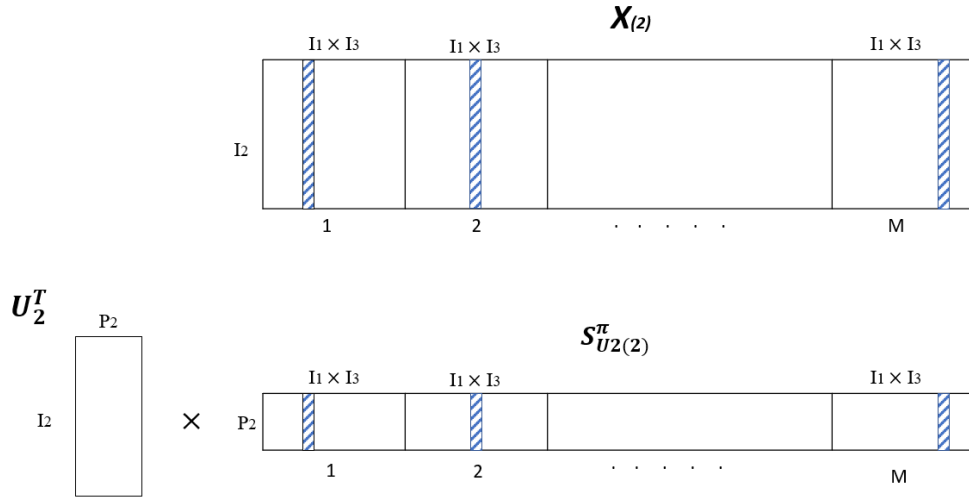


Figure 17: An illustration of the data missing pattern in Proposition 10 (stripes representing available columns).

It can be easily shown that \mathcal{X} 's mode-2 matricization $\mathbf{X}_{(2)}$ has missing columns as well (see Figure 17 for an illustration). Therefore, similar to the proof of Proposition 9, we have $\frac{d}{d\mathbf{U}_2} (\|\mathbf{X}_{(2)}^\pi - \mathbf{U}_2^\top \cdot \mathbf{S}_{U_2(2)}^\pi\|_F^2) = \mathbf{0}$, where π denotes the indices of available columns in $\mathbf{X}_{(2)}$, $\mathbf{S}_{U_2(2)}^\pi$ denotes a matrix constituting the π columns of $\mathbf{S}_{U_2(2)}$. As a result, we have $2(\mathbf{X}_{(2)}^\pi - \mathbf{U}_2^\top \cdot \mathbf{S}_{U_2(2)}^\pi) \cdot (-\mathbf{S}_{U_2(2)}^{\pi \top}) = \mathbf{0}$. Thus, $\mathbf{U}_2^\top \cdot \mathbf{S}_{U_2(2)}^\pi \cdot \mathbf{S}_{U_2(2)}^{\pi \top} = \mathbf{X}_{(2)}^\pi \cdot \mathbf{S}_{U_2(2)}^{\pi \top}$, which gives that $\mathbf{U}_2^\top = \mathbf{X}_{(2)}^\pi \cdot \mathbf{S}_{U_2(2)}^{\pi \top} \cdot (\mathbf{S}_{U_2(2)}^\pi \cdot \mathbf{S}_{U_2(2)}^{\pi \top})^{-1}$. This yields the analytical solution $\mathbf{U}_2 = (\mathbf{X}_{(2)}^\pi \cdot \mathbf{S}_{U_2(2)}^{\pi \top} \cdot (\mathbf{S}_{U_2(2)}^\pi \cdot \mathbf{S}_{U_2(2)}^{\pi \top})^{-1})^\top$.

References

- Abdi, H. and L. J. Williams (2010). Principal component analysis. *Wiley interdisciplinary reviews: computational statistics* 2(4), 433–459.
- Aydemir, G. and K. Paynabar (2019). Image-based prognostics using deep learning approach. *IEEE Transactions on Industrial Informatics* 16(9), 5956–5964.
- Bogdanoff, J. L. and F. Kozin (1985). Probabilistic models of cumulative damage(book). *New York, Wiley-Interscience, 1985, 350 p.*
- Dong, Y., T. Xia, D. Wang, X. Fang, and L. Xi (2021). Infrared image stream based regressors for contactless machine prognostics. *Mechanical Systems and Signal Processing* 154, 107592.
- Doray, L. (1994). Ibrn reserve under a loglinear location-scale regression model. In *Casualty Actuarial Society Forum*, Volume 2, pp. 607–652. Citeseer.
- Fang, X., K. Paynabar, and N. Gebraeel (2019). Image-based prognostics using penalized tensor regression. *Technometrics* 61(3), 369–384.
- Filipović, M. and A. Jukić (2015). Tucker factorization with missing data with application to low-n-rank tensor completion. *Multidimensional systems and signal processing* 26(3), 677–692.
- Gebraeel, N., A. Elwany, and J. Pan (2009). Residual life predictions in the absence of prior degradation knowledge. *IEEE Transactions on Reliability* 58(1), 106–117.
- Gebraeel, N. Z., M. A. Lawley, R. Li, and J. K. Ryan (2005). Residual-life distributions from component degradation signals: A bayesian approach. *IIE Transactions* 37(6), 543–557.
- Hong, Y. and W. Q. Meeker (2010). Field-failure and warranty prediction based on auxiliary use-rate information. *Technometrics* 52(2), 148–159.
- Hong, Y. and W. Q. Meeker (2013). Field-failure predictions based on failure-time data with dynamic covariate information. *Technometrics* 55(2), 135–149.

- Jiang, Y., T. Xia, D. Wang, X. Fang, and L. Xi (2022). Adversarial regressive domain adaptation framework for infrared thermography-based unsupervised remaining useful life prediction. *IEEE Transactions on Industrial Informatics*.
- Kolda, T. G. (2006). Multilinear operators for higher-order decompositions. Technical report, Citeseer.
- Kolda, T. G. and B. W. Bader (2009). Tensor decompositions and applications. *SIAM review* 51(3), 455–500.
- Liu, J., P. Musialski, P. Wonka, and J. Ye (2012). Tensor completion for estimating missing values in visual data. *IEEE transactions on pattern analysis and machine intelligence* 35(1), 208–220.
- Liu, K., N. Z. Gebraeel, and J. Shi (2013). A data-level fusion model for developing composite health indices for degradation modeling and prognostic analysis. *IEEE Transactions on Automation Science and Engineering* 10(3), 652–664.
- Lu, H., K. N. Plataniotis, and A. N. Venetsanopoulos (2008). Mpca: Multilinear principal component analysis of tensor objects. *IEEE transactions on Neural Networks* 19(1), 18–39.
- Prautzsch, H., W. Boehm, and M. Paluszny (2002). *Bézier and B-spline techniques*, Volume 6. Springer.
- Ramsay, J. and B. Silverman (2005). Principal components analysis for functional data. *Functional data analysis*, 147–172.
- Shu, Y., Q. Feng, and D. W. Coit (2015). Life distribution analysis based on lévy subordinators for degradation with random jumps. *Naval Research Logistics (NRL)* 62(6), 483–492.
- Tang, D., M. Gong, J. Yu, L. Guo, and J. Di (2021). System-level performance prediction for infrared systems based on energy redistribution in infrared images. *IEEE Transactions on Industrial Electronics* 69(2), 2000–2011.

- Xu, Y., R. Hao, W. Yin, and Z. Su (2013). Parallel matrix factorization for low-rank tensor completion. *arXiv preprint arXiv:1312.1254*.
- Xu, Y. and W. Yin (2013). A block coordinate descent method for regularized multiconvex optimization with applications to nonnegative tensor factorization and completion. *SIAM Journal on imaging sciences* 6(3), 1758–1789.
- Yang, Z., P. Baraldi, and E. Zio (2021). A multi-branch deep neural network model for failure prognostics based on multimodal data. *Journal of Manufacturing Systems* 59, 42–50.
- Ye, Z.-S. and N. Chen (2014). The inverse gaussian process as a degradation model. *Technometrics* 56(3), 302–311.
- Ye, Z.-S., M. Xie, L.-C. Tang, and N. Chen (2014). Semiparametric estimation of gamma processes for deteriorating products. *Technometrics* 56(4), 504–513.